

ORIGINAL ARTICLE

Immunomodulatory fibrous hyaluronic acid-Fmoc-diphenylalanine-based hydrogel induces bone regeneration

Michal Halperin-Sternfeld^{1,2,3}  | Ariel Pokhojaev¹ | Moumita Ghosh^{1,2,3,4} |
 Dana Rachmiel^{1,2,3} | Raha Kannan⁵ | Itzhak Grinberg^{1,2,3} | Moshe Asher¹ |
 Moran Aviv^{1,2,3,6} | Peter X. Ma⁵ | Itzhak Binderman¹  | Rachel Sarig^{1,7}  |
 Lihi Adler-Abramovich^{1,2,3} 

¹Department of Oral Biology, The Maurice and Gabriela Goldschleger School of Dental Medicine, Sackler Faculty of Medicine, Tel Aviv University, Tel Aviv, Israel

²The Center for Nanoscience and Nanotechnology, Tel Aviv University, Tel Aviv, Israel

³The Center for the Physics and Chemistry of Living Systems, Tel Aviv University, Tel Aviv, Israel

⁴Department of Chemistry, Techno India University, Kolkata, West Bengal, India

⁵Department of Biologic and Materials Sciences, University of Michigan, Ann Arbor, Michigan, USA

⁶School of Mechanical Engineering, Afeka Tel Aviv Academic College of Engineering, Tel Aviv, Israel

⁷The Dan David Center for Human Evolution and Biohistory Research, Tel Aviv University, Tel Aviv, Israel

Correspondence

Rachel Sarig and Lihi Adler-Abramovich,
 Department of Oral Biology, The Maurice and
 Gabriela Goldschleger School of Dental
 Medicine, Sackler Faculty of Medicine, Tel
 Aviv University, Tel Aviv 6997801, Israel.
 Email: sarigrac@tauex.tau.ac.il and lihia@tauex.
 tau.ac.il

Funding information

Clore Duffield Foundation; GRTF travel grant;
 H2020 European Research Council,
 Grant/Award Number: 948102; Israel Science
 Foundation, Grant/Award Number: 1732/17;
 United States - Israel Binational Science
 Foundation, Grant/Award Number: 2018102;
 Ministry of Science, Technology & Space, Israel

Abstract

Aim: To investigate the potential of an ultrashort aromatic peptide hydrogelator integrated with hyaluronic acid (HA) to serve as a scaffold for bone regeneration.

Materials and Methods: Fluorenylmethyloxycarbonyl-diphenylalanine (FmocFF)/HA hydrogel was prepared and characterized using microscopy and rheology. Osteogenic differentiation of MC3T3-E1 preosteoblasts was investigated using Alizarin red, alkaline phosphatase and calcium deposition assays. In vivo, 5-mm-diameter calvarial critical-sized defects were prepared in 20 Sprague–Dawley rats and filled with either FmocFF/HA hydrogel, deproteinized bovine bone mineral, FmocFF/Alginate hydrogel or left unfilled. Eight weeks after implantation, histology and micro-computed tomography analyses were performed. Immunohistochemistry was performed in six rats to assess the hydrogel's immunomodulatory effect.

Results: A nanofibrous FmocFF/HA hydrogel with a high storage modulus of 46 KPa was prepared. It supported osteogenic differentiation of MC3T3-E1 preosteoblasts and facilitated calcium deposition. In vivo, the hydrogel implantation resulted in approximately 93% bone restoration. It induced bone deposition not only around the margins, but also generated bony islets along the defect. Elongated M2 macrophages lining at the periosteum–hydrogel interface were observed 1 week after implantation. After 3 weeks, these macrophages were dispersed through the regenerating tissue surrounding the newly formed bone.

This is an open access article under the terms of the [Creative Commons Attribution-NonCommercial-NoDerivs](https://creativecommons.org/licenses/by-nc-nd/4.0/) License, which permits use and distribution in any medium, provided the original work is properly cited, the use is non-commercial and no modifications or adaptations are made.

© 2022 The Authors. *Journal of Clinical Periodontology* published by John Wiley & Sons Ltd.

Conclusions: FmocFF/HA hydrogel can serve as a cell-free, biomimetic, immunomodulatory scaffold for bone regeneration.

KEYWORDS

biomaterials, bone regeneration, hyaluronic acid, immunomodulation, self-assembling peptides

Clinical Relevance

Scientific rationale for study: Biomimetic materials that can stimulate and accelerate bone formation without embedding cells and growth factors are of great importance in bone tissue engineering.

Principal findings: FmocFF/hyaluronic acid (HA) hydrogel is a stiff extracellular matrix-biomimetic hydrogel that supports complete regeneration of the rat calvaria's original thickness and density. An osteoimmunomodulatory effect of the hydrogel on the periosteum leading to macrophage recruitment to the hydrogel where they differentiate early into M2 macrophages that promote angiogenesis and osteogenesis is suggested.

Practical implications: Large bone defects may be restored by the use of the organic FmocFF/HA hydrogel.

1 | INTRODUCTION

Reconstruction of bone defects that cannot heal spontaneously, that is, critical-sized bone defects, continues to be an enormous clinical challenge. Such defects may result from trauma, inflammation or following bone tumour resections. Although autogenic, allogeneic and xenogeneic bone materials have been widely applied to treat such defects, they possess potential limitations (Stevens, 2008), including limited availability and donor site morbidity (Silber et al., 2003), potential immunogenicities (H. Zhang et al., 2019) and risk for disease transmission (Shao et al., 2018).

The classic tissue engineering approach, involving the use of living cells, growth factors and a basic scaffold, has emerged as a promising tool to address these issues (Vacanti & Langer, 1999). However, despite the undoubted potential held by this approach, it still involves ex vivo cell manipulation, which may have immunogenic and tumorigenic potential (Heslop et al., 2015). An alternative tissue engineering strategy that eliminates the need for exogenous cells is developing cell-free scaffolds that can utilize the recipient's endogenous cells for in situ tissue regeneration. Such scaffolds are designed to mimic the ability of the natural extracellular matrix (ECM) to effectively recruit host cells to the defect site while providing structural support for the recruited cells to promote angiogenesis and osteogenesis (Franz et al., 2011).

Hydrogels are of particular interest as cell-ingrowth scaffolds for tissue engineering and bone regeneration, as they offer a three-dimensional (3D) network for cell attachment and growth (Bai et al., 2018; Cheng et al., 2020; Derkus et al., 2020). Specifically, naturally occurring polysaccharides, including hyaluronic acid (HA), alginate (Alg) and chitosan, have elicited an immense amount of attention due to their high biocompatibility, biodegradability, low immunogenicity and abundance in nature (Witzler et al., 2019). Nevertheless, their usefulness has been limited by unsatisfactory mechanical properties

and a high degradation rate (Stevens, 2008). To overcome these drawbacks, polysaccharides are often chemically cross-linked (Witzler et al., 2019).

An alternative method to strengthen polysaccharides is by integrating them with self-assembling short peptide hydrogelators to create composite hydrogels with improved and tunable mechanical properties (Gong et al., 2016; Aviv et al., 2018; Ghosh et al., 2019; Halperin-Sternfeld et al., 2022). Self-assembling short peptides are peptides comprising less than eight amino acids that undergo molecular self-assembly. Well-defined and stable macroscopic structures are produced by the spontaneous organization of the peptides and are held together by non-covalent interactions, including aromatic π - π stacking interactions, hydrogen bonding, van der Waals forces, and electrostatic and hydrophobic interactions (S. Zhang, 2003; L. Wang et al., 2019). The synergy between these weak collective interactions provides the basis for these structures' chemical and structural stability (S. Zhang et al., 2002). The advantages of the self-assembling peptides are the ease and relatively low cost of synthesis, chemical diversity, high stability and biocompatibility (Yadav et al., 2020). These attributes render them attractive candidates for various applications such as cell culture (Dou & Feng, 2017; Diaferia et al., 2020), tissue engineering and drug delivery (Hartgerink et al., 2002; Kisiday et al., 2002; S. Zhang, 2003; Beniash et al., 2005; Kretsinger et al., 2005; Jayawarna et al., 2006; Dou & Feng, 2017; Yadav et al., 2020; Rachmiel et al., 2021), fabric functionalization (Khadeja et al., 2019), bio-imaging (Diaferia, Gianolio, & Accardo, 2019; Ni et al., 2019; Gallo et al., 2020) and 3D printing (Netti et al., 2022).

Self-supporting hydrogels formed by self-assembly of short peptides modified with aromatic groups such as 9-fluorenylmethoxycarbonyl (Fmoc) (Y. Zhang et al., 2003; Jayawarna et al., 2006; Mahler et al., 2006; Smith et al., 2008; Adams et al., 2009, 2010; Zhou et al., 2009; Fichman & Gazit, 2014; Brito et al., 2019; Debnath et al., 2019; Draper & Adams, 2019) have been proposed for use in

various biological applications, including cell culture (Jayawarna et al., 2006, 2009), tissue engineering (Y. Wang et al., 2013; Deidda et al., 2017; Brito et al., 2019), antigen presentation (Vegners et al., 1995), anti-infective biomaterials (McCloskey et al., 2017) and drug delivery (Huang et al., 2011; Ischakov et al., 2013). One of the most studied short aromatic peptides is FmocFF, a dipeptide protected by an aromatic group that can self-assemble into fibrillar hydrogels (Jayawarna et al., 2006; Mahler et al., 2006; Smith et al., 2008; Raeburn et al., 2012; Diaferia, Morelli, & Accardo, 2019; Tikhonova et al., 2021). In the case of FmocFF and other ultrashort peptides containing aromatic residues, π - π interactions are the most dominant interactions that stabilize the self-assembly process into 3D hydrogels (Smith et al., 2008).

FmocFF has recently been used in combination with other materials such as polysaccharides, proteins and peptides to form hybrid systems (Huang et al., 2011; Celik et al., 2016; Gong et al., 2016; Ghosh et al., 2017, 2019; Halperin-Sternfeld et al., 2017, 2022; Aviv et al., 2018; Diaferia, Morelli, & Accardo, 2019; Netti et al., 2022). Specifically, combining FmocFF with polysaccharides enabled the formation of stable hydrogels without the need for cross-linking agents (Huang et al., 2011; Gong et al., 2016; Aviv et al., 2018; Ghosh et al., 2019; Halperin-Sternfeld et al., 2022). Huang et al. (2011) fabricated a composite hydrogel from FmocFF and the polysaccharide, konjac glucomannan, for the sustained delivery of hydrophobic drugs. The composite hydrogel had a nanofibrous architecture and displayed high rigidity when compared with FmocFF alone (Huang et al., 2011). A similar improvement in the mechanical properties was observed when FmocFF was integrated with Alg and HA to form composite hydrogels (Aviv et al., 2018; Ghosh et al., 2019). Also, the FmocFF/Alg composite hydrogel could induce osteogenic differentiation of MC3T3-E1 preosteoblasts and facilitate calcium mineralization. This capacity is probably due to the high rigidity, as it has been well established that the hydrogel's mechanical stiffness directs stem cell differentiation (Alakpa et al., 2016).

We have recently developed FmocFF/HA composite hydrogels with tunable mechanical properties where we could fabricate hydrogels with different rigidity and degradation rates by changing the components' concentration (Aviv et al., 2018). Increasing the peptide concentration within the hydrogels resulted in higher rigidity and a lower degradation rate. The higher rigidity may be attributed to the high density and the compact nanostructure of the hydrogel comprising entangled fibrils. Moreover, the compact structure of the composite hydrogel may hinder the penetration of hyaluronidase, the enzyme responsible for HA degradation, thus decreasing the hydrogel degradation rate (Aviv et al., 2018). We have demonstrated these hydrogels' potential to serve as vehicles for the controlled release of biomolecules, including curcumin. Furthermore, the hydrogels were biocompatible and supported the adherence of fibroblasts (Aviv et al., 2018).

HA has been widely used in bone regenerative medicine, particularly in maxillofacial and periodontal surgeries (Eliezer et al., 2019; Zhai et al., 2020), since it is biocompatible, biodegradable, non-toxic, non-immunogenic and non-inflammatory. As a naturally occurring non-sulphated glycosaminoglycan found in the ECM of most

connective tissues (Chircov et al., 2018), it can serve as a biomimetic extracellular environment for cell adhesion, proliferation and differentiation through the cellular surface marker CD44 (Hemshekhar et al., 2016). High molecular weight HA (>500 kDa) predominates in normal tissues (Liu et al., 2019). Its metabolism is regulated by three synthases (HAS 1-3) and three hyaluronidases (HYAL 1-3) (Kobayashi et al., 2020). The different HAS control HA synthesis at multiple stages, and the different hyaluronidases are in charge of its degradation in different locations. Hyaluronidase 1 and 3 are enzymes located mainly in lysosomes and, together with glucosaminidase and glucuronidase, degrade HA into monomers (Csoka et al., 2001), while Hyaluronidase 2 is located at the cell surface and, together with extracellular reactive oxygen/nitrate (ROS/NOS), degrades the high molecular weight HA into low molecular weight HA (Monzon et al., 2010). Recently, cell migration inducing protein (CEMIP)/KIAA1199 and transmembrane protein 2 (TMEM2) have also been found to be involved in extracellular HA degradation (Yoshida et al., 2013; Yamamoto et al., 2017). Ideally, scaffolds for tissue engineering and regenerative applications should degrade through the course of tissue regeneration. Since HA has poor mechanical properties and rapid degradation, it is often chemically and physically modified by cross-linking agents to improve its mechanical properties (Wende et al., 2016; Tiwari & Bahadur, 2019). Furthermore, it has been integrated with inorganic materials such as hydroxyapatite, tricalcium phosphate, tendon tissue or demineralized bone matrix to form scaffolds that have been shown to enhance osteogenesis (Zhai et al., 2020). Exploiting the ability of FmocFF to self-assemble spontaneously into a nanofibrous structure, it was used to physically strengthen HA without the need of a cross-linking agent to yield transparent self-supporting rigid hydrogels (Aviv et al., 2018).

Here, we explore the ability of the FmocFF/HA composite hydrogel to promote bone regeneration as an organic matrix without the use of cross-linking agents or inorganic materials. To this end, we fabricated a composite hydrogel and studied its structural and mechanical properties using electron microscopy, rheology and Fourier-transform infrared (FTIR) spectroscopy. We further assessed its ability to induce osteodifferentiation and biomineralization *in vitro* using MC3T3-E1 preosteoblasts. Finally, we tested the ability of the hydrogel to induce regeneration of critical-sized bone defects covered by periosteum in a rat model *in vivo* and explored its mechanism.

2 | MATERIALS AND METHODS

2.1 | Materials

Lyophilized FmocFF peptide was purchased from Bachem (Budendorf, Switzerland) and high molecular weight (3×10^6 Da) sodium hyaluronate 10 mg/ml in phosphate-buffered saline syringes were purchased from BTG-Ferring (Kiryat Malachy, Israel). Sodium alginate (molecular weight 240 kDa, viscosity 15-25 cP, 1% in H₂O), 3-[4,5-dimethylthiazole-2-yl]-2,5-diphenyltetrazolium bromide (MTT), fluorescein diacetate, propidium iodide, 4-Methylumbelliferyl phosphate (4-MUP), Alizarin red and 9-mm-

diameter \times 2-mm-depth silicone isolators were purchased from Sigma-Aldrich Inc. (Rehovot, Israel). Calcium Reagent Set was purchased from Pointe Scientific (USA). Dulbecco's Modified Eagle's Medium (DMEM), Minimum Essential Media Alpha, fetal bovine serum, fetal calf serum (FCS), penicillin and streptomycin were purchased from Biological Industries (Beit-Haemek, Israel).

2.2 | Structural and mechanical characterization of the FmocFF/HA hydrogel

2.2.1 | FmocFF/HA composite hydrogel preparation

Exactly 125 mg of HA in phosphate-buffered saline (10 mg/ml) was mixed with 850 μ l double distilled water (ddH₂O) using a shaker overnight. FmocFF stock solution was prepared by dissolving the peptide in dimethyl sulfoxide (DMSO) solvent (150 mg peptide in 1 ml of DMSO) by vortexing until a transparent solution was obtained. Peptide stock solution (25 μ l) was then added to the mixture of HA in ddH₂O and vortexed. The final concentration of the hydrogel was 5 mg/ml (3.75 mg of FmocFF and 1.25 mg of HA in 1 ml of solution) with 2.5% DMSO.

2.2.2 | Transmitting electron microscopy

FmocFF/HA composite hydrogel (10 μ l) was placed on a 400-mesh copper grid and excess fluid was removed. Negative staining was achieved by the deposition of 10 μ l of 2% uranyl acetate in water. After 2 min, excess uranyl acetate was removed. The sample was viewed using a JEM-1400Plus Transmission Electron Microscope (JEM), operating at 80 kV.

2.2.3 | Scanning electron microscopy

A sample of FmocFF/HA composite hydrogel was placed on a metal stand, freeze-dried and lyophilized, and then coated with a thin gold layer and viewed by scanning electron microscopy (SEM) (JEOL, JSM-IT100 InTouchScope™) operating at 20 kV.

2.2.4 | FTIR spectroscopy

FTIR spectra were collected 4 days after hydrogel preparation using a Nicolet Nexus 470 FTIR spectrometer with a DTGS (deuterated triglycine sulphate) detector. Hydrogel samples were placed onto disposable KBr IR sample cards (Sigma-Aldrich) and vacuum dried. Measurements were performed using 4 cm⁻¹ resolution and by averaging 2000 scans. The absorbance maxima values were determined using the OMNIC analysis program (Nicolet). The obtained transmittance spectra were smoothed by applying the Savitzky-Golay

function to eliminate noise and operating the second derivative transformation on the spectra using Peakfit software version 4.12 (SYSTAT Software Inc., Richmond, CA).

2.2.5 | Rheological studies

The mechanical properties of the hydrogel were studied with an AR-G2 rheometer (TA Instruments, New Castle, DA) equipped with a Stainless Steel 20-mm-diameter parallel-plate geometry. Oscillatory strain (0.01%–100%), frequency sweep (0.01–100 Hz) and shear rate (0.01–100/s) tests were conducted to determine the linear viscoelastic region on 240- μ l freshly prepared hydrogel (resulting in a gap size of 0.6 mm) at 37°C. A time-sweep oscillatory test was performed at 5 Hz oscillation and 0.1% strain deformation to determine G' and G'' , namely the storage and loss moduli, respectively. The self-healing behaviour of the hydrogel was tested under a cyclic high (100%) and low (0.1%) strain at a constant frequency of 5 Hz.

2.3 | In vitro biological assays for assessment of MC3T3-E1 preosteoblasts migration within the hydrogel and osteogenic differentiation

All biological assays were performed in triplicate, with five replicates per experiment.

2.3.1 | Migration of MC3T3-E1 preosteoblasts within the hydrogel

To assess the adherence and migration of cells, the hydrogels were prepared using a 9-mm-diameter \times 2-mm-depth silicone mould containing a final volume of 90 μ l, placed in a 35-mm glass-bottom dish and repeatedly washed with culture medium for 3 days, followed by UV sterilization for 30 min. After sterilization, MC3T3-E1 preosteoblasts (20,000 cells per 100 μ l) were seeded on the hydrogel. After 1 day, the cells were stained with fluorescein diacetate (6.6 μ g/ml) for 5 min at room temperature to identify cell attachment and migration. The cells were imaged using a Leica SP8 X Confocal Microscope.

2.3.2 | Mineralization assay using Alizarin red

Osteogenic differentiation of MC3T3-E1 preosteoblasts on the FmocFF/HA hydrogel was evaluated by the Alizarin red quantification assay and compared with cells seeded on the plate. FmocFF/HA hydrogels were formed in a 24-well plate and repeatedly washed with culture media for 3 days, followed by UV sterilization for 30 min. A total of 50,000 MC3T3-E1 preosteoblasts per 100 μ l were seeded on the prewashed hydrogels and incubated at 37°C in a humidified atmosphere under 5% CO₂. After 2 days, the cells were supplemented with osteogenic media containing ascorbic acid and beta-

glycerophosphate. The cells were maintained in osteogenic media for 14 days with the media replaced every 2 days. After 14 days, the cells were stained with the calcium staining dye Alizarin red. Calcium deposits could be visualized by their red colour under a light microscope. After washing off the excess dye, optical light microscopy images were acquired. Then, the deposited calcium was extracted by AcOH/MeOH (1:2) buffer. The absorbance at 450 nm was assessed for each well with and without differentiation after subtracting the background binding to the hydrogel itself, and normalized to the cell count. The normalization was performed by counting the number of cells in each well based on cells' nuclei staining with DAPI and fluorescence measurements at 360 nm. The quantification was done using the following formula:

$$\text{Normalized absorbance} = \frac{\text{Alizarin red absorbance}}{\text{DAPI fluorescence}} \times 10,000$$

2.3.3 | Alkaline phosphatase activity

To determine the cellular alkaline phosphatase (ALP) activity, FmocFF/HA hydrogels were formed in a 24-well plate and repeatedly washed with culture medium for 3 days, followed by UV sterilization for 30 min. A total of 50,000 MC3T3-E1 preosteoblasts per 100 μ l were seeded on the prewashed hydrogels. After 2 days, the cells were supplemented with osteogenic media containing ascorbic acid and beta-glycerophosphate. The cells were maintained in osteogenic media for 14 days with the media replaced every 2 days. After 14 days, the hydrogels were stained with 100 μ l ALP substrate solution containing pNPP and incubated away from light at 37°C for 30 min. The absorbance at 405 nm was read for each well with and without differentiation and normalized by the number of cells. The normalization was performed by counting the number of cells in each well based on cells' nuclei staining with DAPI and fluorescence measurements at 360 nm. The quantification was done using the following formula:

$$\text{Normalized absorbance} = \frac{\text{ALP absorbance}}{\text{DAPI Fluorescence}} \times 10,000$$

2.3.4 | Calcium deposition on the FmocFF/HA hydrogel

FmocFF/HA hydrogels were formed in a 24-well plate and repeatedly washed with culture medium for 3 days, followed by UV sterilization for 30 min. A total of 50,000 MC3T3-E1 preosteoblasts per 100 μ l were seeded on the prewashed hydrogels in osteogenic media containing ascorbic acid and beta-glycerophosphate. Cells were maintained in osteogenic media for 14 days with the media replaced every 2 days. Following 14 days of induced osteogenic

differentiation, the hydrogels were treated with 0.5 N HCl in a cold room (4°C) on a shaker for 24 h. After 24 h, calcium present in the acidic supernatant was quantified using a commercially available kit (Calcium Reagent Set, Pointe Scientific) following the manufacturer's instructions. Light absorbance of the acidic supernatant solution with the addition of a calcium reagent was read at 570 nm. Calcium content was determined from a standard curve of absorbance against a known concentration of calcium run in parallel with the acidic supernatant solution. Results were normalized over the hydrogel surface area.

2.4 | In vivo evaluation of the composite FmocFF/HA hydrogel's biocompatibility in a rat subcutaneous model and its effect on bone regeneration in a calvarial critical-sized defect model

2.4.1 | Hydrogel preparation

For the in vivo study, FmocFF/HA hydrogels were prepared using the same protocol and then transferred to one end-closed tubular dialysis membranes 6 mm in diameter (CelluSep® T3 tubing, 12,000–14,000 MWCO). The other end of the membranes was appropriately closed, and the samples were submerged in 20 ml of DMEM containing 10% FCS and 100 U/ml penicillin, 200 mM L-glutamine in capped 50 ml Falcon® tubes. The medium was replaced eight times over 3 days before surgery in order to eliminate residual FmocFF monomers and DMSO.

FmocFF/Alg hydrogel was prepared as previously described (Ghosh et al., 2019), transferred into dialysis bags similar to the FmocFF/HA hydrogel and washed with DMEM for 3 days.

2.4.2 | Biocompatibility analysis of the hydrogel in a rat subcutaneous model

The surgical and animal care procedure was reviewed and approved by the committee for the Supervision of Animal Experiments at Tel Aviv University (approval #01-17-078), in compliance with the guidelines for animal experimentation of the National Institutes of Health. FmocFF/HA hydrogels were prepared and soaked with bone marrow harvested from the femur of homologous individuals. A subcutaneous pouch was created by a U-shaped incision using a scalpel in the chest of the rats. Simultaneously, bone marrow was harvested from homologous individuals. After euthanization, both ends of the bilateral femora of syngeneic rats were cut, and bone marrow plugs were retrieved. The hydrogel was soaked in the bone marrow in a Petri dish. Then, the hydrogel was placed in the subcutaneous pouch, and the incision were sutured. After 4 weeks, the implant was harvested and placed in ethanol. After decalcification, histologic sections were stained for haematoxylin and eosin (H&E) and imaged using a light microscope (Olympus DP70, Tokyo, Japan).

2.4.3 | Rat calvarial bone defect model

Surgical and animal care procedures were reviewed and approved by the committee for the Supervision of Animal Experiments at Tel Aviv University (approval #01-18-041), in compliance with the guidelines for animal experimentation of the National Institutes of Health. A minimal number of rats were used, and all efforts were made to minimize potential suffering.

Twenty 8-week old female Sprague-Dawley rats with pre-operative weights ranging from 200 to 250 g (Envigo, Israel) were involved. The animals were anaesthetised through intra-peritoneal injection of ketamine (100 mg/kg) and xylazine (5 mg/kg), followed by subcutaneous enrofloxacin 5% (5 mg/kg) to minimize the risk of infection, and Rimadyl (5 mg/kg) for pain management. Local anaesthesia was administered using 2% lidocaine with 1/100,000 epinephrine. The dorsal part of the cranium was shaved and aseptically prepared with 1% iodine. A U-shaped incision was made, and a full-thickness flap was reflected, exposing the parietal and frontal bones. A critical-size defect of 5 mm diameter was created in the right parietal bone of each rat with a trephine bur under saline irrigation, leaving the left parietal bone intact serving as a control. Care was taken not to damage the dura mater during the surgery. The rats were randomly divided into four groups ($n = 5$). Each defect was filled with either FmocFF/HA hydrogel, FmocFF/Alg hydrogel or small particles (0.25–1 mm) of deproteinized bovine bone mineral (BBM) (Bio-Oss[®], Geistlich Pharma, Wolhusen, Switzerland) as a positive control, or left unfilled as a negative control. Surgical flaps were re-positioned, and three single interrupted 5–0 Nylon sutures were placed. The animals were euthanized 8 weeks post-surgery by CO₂ asphyxiation, and the calvarias were harvested. The specimens were immediately fixed in 4% paraformaldehyde for 48 h and then placed in 70% ethanol.

2.4.4 | Micro-computed tomography analysis

All specimens were scanned using a Scanco micro-computed tomography (micro-CT) 50 system (Scanco Medical AG, Switzerland). Scans were performed at an isotropic resolution of 17.2 μm utilizing the following parameters: 34 mm tube, 90 kVp energy, at 200 μA intensity, Al 0.5 mm filter and with 1000 projections at a 1000 ms integration time. The images were 3D reconstructed in Amira software (v 6.3, www.fei.com) for analysis. A 5-mm-diameter circular region of interest (ROI) was analysed. A corresponding 5 mm circular area in the left parietal bone of each rat served as a control and as a reference for calculations. A colour map demonstrating the restored bone thickness in the defect and the corresponding control circular area was drawn. The restored bone volume was calculated as the ratio between the right (experimental) and left (control) ROIs and presented as a percentage. The 5-mm circular defect was then virtually divided into three regions with equal volumes, namely, outer, middle and inner, and the restored bone volume in each region was calculated and compared between the three regions. The restored bone density in the defined ROIs was calculated from the grayscale values of the micro-CT scans using a calibration phantom provided by the manufacturer (Scanco Medical AG). The ratio between the newly formed bone density to the bone density of the control side was presented as a percentage. All the

specimens comprising BBM were segmented using various semi-automatic thresholding tools in Amira software to morphologically separate visible BBM particles from the surrounding bone.

2.4.5 | Histological preparation

Specimens comprising FmocFF/HA hydrogel, FmocFF/Alg hydrogel and unfilled defects were fixed with 4% paraformaldehyde and decalcified with 10% EDTA for 21 days. They were then sliced across the centre of the defect, embedded in paraffin and sectioned into 5- μm -thick slices. Bone morphology was visualized by H&E and Masson's trichrome stains. Analysis was performed using a light microscope (Olympus BX-50, Tokyo, Japan) and photomicrographs were acquired using a camera mounted on the microscope (Olympus DP70).

2.5 | Immunohistochemistry for the assessment of the in vivo osteoimmunomodulatory effect of FmocFF/HA hydrogel

Eighteen rats were included in this study using the abovementioned protocol. Exactly 1 and 3 weeks after the implantation of either FmocFF/HA hydrogel, BBM and unfilled defects, three rats from each group were euthanized and the calvarias were harvested. The specimens were immediately fixed in 4% paraformaldehyde for 48 h and then placed in 70% ethanol. Decalcification was performed with 10% EDTA for 21 days. The specimens were sliced across the centre of the defect, embedded in paraffin and sectioned into 5- μm -thick slices. The slices were stained with haematoxylin and then labelled with either CD68 or CD163 to determine M1 and M2 macrophage phenotypes, respectively. The slides were scanned in Aperio VERSA Brightfield Digital Scanner (Leica Biosystems, Buffalo Grove, IL) and photomicrographs were taken using Aperio ImageScope—Pathology Slide Viewing Software. M1 and M2 macrophage populations were later quantified and compared between the different mice groups 1 and 3 weeks after implantation using the Image J software. The percentage of M1 and M2 macrophages was quantified in three areas on each slide and averaged, and later compared within the three groups.

Statistical analysis was performed using GraphPad Prism Software (GraphPad Software, Inc., San Diego, CA). Data for each assay were analysed with two-tailed Student's *t*-test for comparison between two groups or one-way analysis of variance (ANOVA) with Tukey's post-test for multiple comparisons to examine the effect of the hydrogel and the controls on the parameters investigated. For all tests, statistical significance was set at $p = .05$.

3 | RESULTS

3.1 | Characterization of the FmocFF/HA hydrogel

The FmocFF/HA composite hydrogel was formed by incorporating FmocFF (Figure 1a) into HA (Figure 1b) to a final concentration of

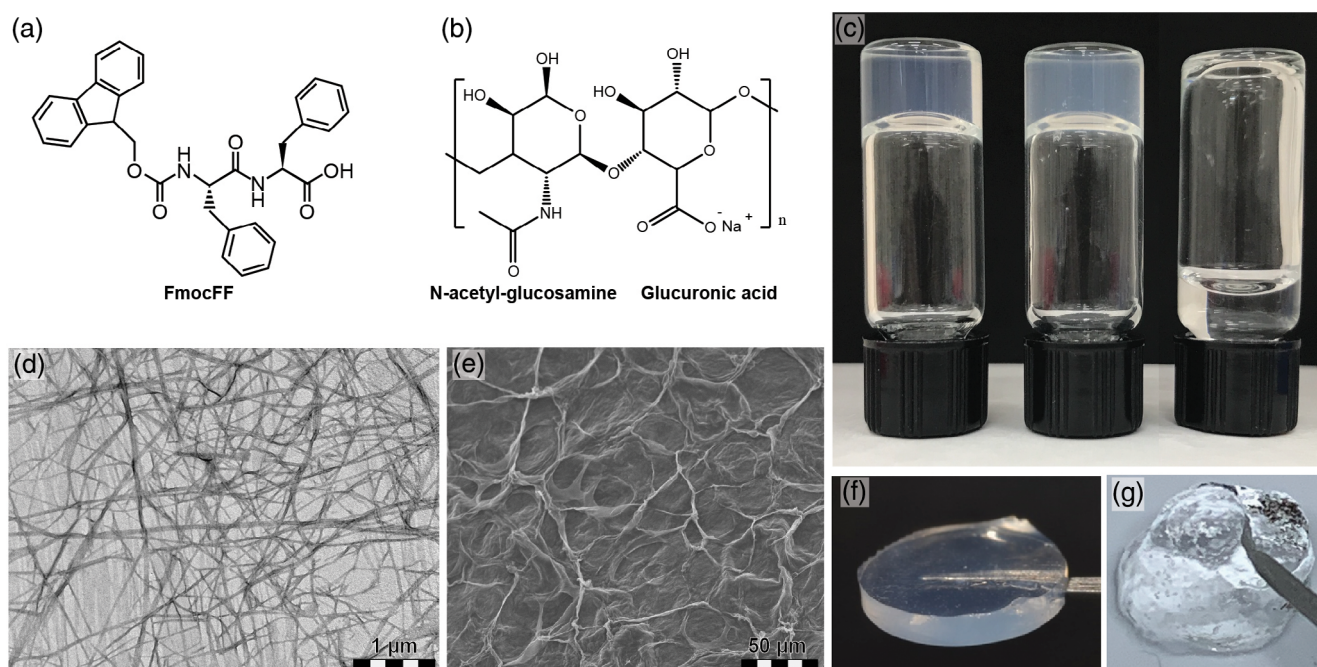


FIGURE 1 FmocFF/hyaluronic acid (HA) composite hydrogel formation and structural characterization. (a) Molecular structure of the FmocFF peptide. (b) Molecular structure of HA. (c) Inverted vials of FmocFF (left), FmocFF/HA composite hydrogel (middle) and HA (right). (d) Transmitting electron microscopy micrograph of the FmocFF/HA composite hydrogel. (e) Scanning electron microscopy micrograph of the FmocFF/HA composite hydrogel. (f) The FmocFF/HA composite hydrogel was formed in a 9 mm diameter \times 2 mm depth silicone mould. (g) The FmocFF/HA composite hydrogel is injected through a 27-gauge needle.

5 mg/ml (Aviv et al., 2018). This gave rise to a self-supported, homogeneous hydrogel formed within a few minutes (Figure 1c). Transmitting electron microscopy and SEM analyses demonstrate the nanofibrillar architecture of the composite hydrogel (Figure 1d,e). The composite hydrogel is mouldable and easy to handle. It can be customized to different configurations (Figure 1f) or applied through a syringe (Figure 1g).

FTIR spectra were measured for the FmocFF/HA composite hydrogel and the individual components (Figure 2a). The distinct peaks observed at 1647 cm^{-1} and at 1694 cm^{-1} are associated with amide I C=O stretching vibration and are directly related to the backbone conformation (Di Foggia et al., 2011). These peaks suggest the presence of a carbamate moiety and indicate that the composite hydrogel is rich in β -sheets. HA showed a peak at 1415 cm^{-1} that corresponds to the presence of a C-O group with C=O combination, and additional peak at 1620 cm^{-1} that indicates Amide II stretching (Kong & Yu, 2007; Di Foggia et al., 2011). These peaks are not visible in the composite hydrogel.

To assess the stiffness of the FmocFF/HA composite hydrogel, we first measured the storage modulus and the loss modulus of the composite hydrogel at dynamic strain sweep (at 5 Hz frequency). To study the effect of oscillatory strain, the hydrogel was subjected to 0.01%–100% strain sweep at a constant frequency, resulting in a broad linear viscoelastic region of up to 5% strain (Figure S1a). Frequency sweep experiments at a constant strain using a frequency range of 0.1–100 Hz also showed a broad linear viscoelastic region (Figure S1b). We determined the linear viscoelastic region based on

both the dynamic strain sweep and frequency sweep tests and conducted a time-sweep measurement at a fixed strain of 0.1% and frequency of 5 Hz. The FmocFF/HA composite hydrogel reached a G' value of 46,425 Pa, which was 9.8-fold higher than the pure FmocFF with a G' of 4708 Pa (Figure 2b). HA alone had a very low G' value of 13 Pa (Figure 2b). Figure 2c shows the viscosity variation of the FmocFF/HA composite hydrogel with respect to shear rate (0.01–100/s). The composite hydrogel showed shear-induced breakage, supporting a shear-thinning behaviour of the gel. At low shear rate, the high viscosity value of the composite hydrogel might have stemmed from the entangled networks of polymer chains and fibrils (Chakraborty et al., 2012). As the shear rate increased, the viscosity value decreased. This is due to the network re-arrangements in the microstructure in the plane of the applied shear. The entanglements were disrupted by the imposed deformation, resulting in the breakage of the fibril network and depletion of the gel. To establish the hydrogel's self-healing nature, an alternate step strain experiment was conducted. The hydrogel was subjected to seven cycles of time-sweep experiments with low (0.1%) and high (100%) strain values (Figure 2d). At 100% strain, the hydrogels were converted to a sol state, as evident from the modulus values ($G' < G''$). When the strain was reduced to 0.1%, the hydrogel recovered ($G' > G''$). This characteristic was consistent over multiple cycles, illustrating the reproducibility of the self-healing nature. The self-healing property of the hydrogel was also observed by the joining of three separate disc hydrogels (Figure 2e,f). Moreover, the recovery of the hydrogel was achieved after applying mechanical force (Figure 3g).

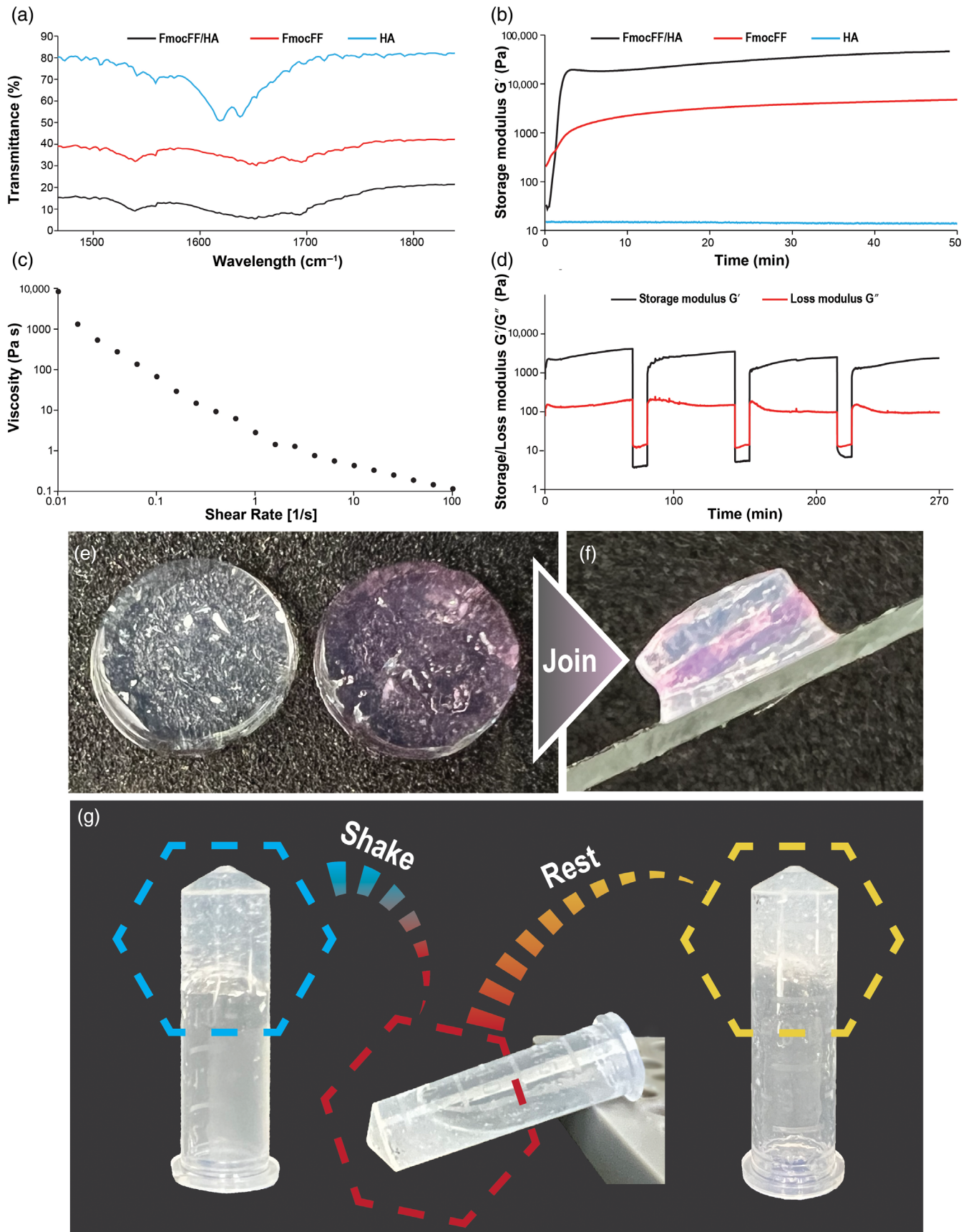


FIGURE 2 Legend on next page.

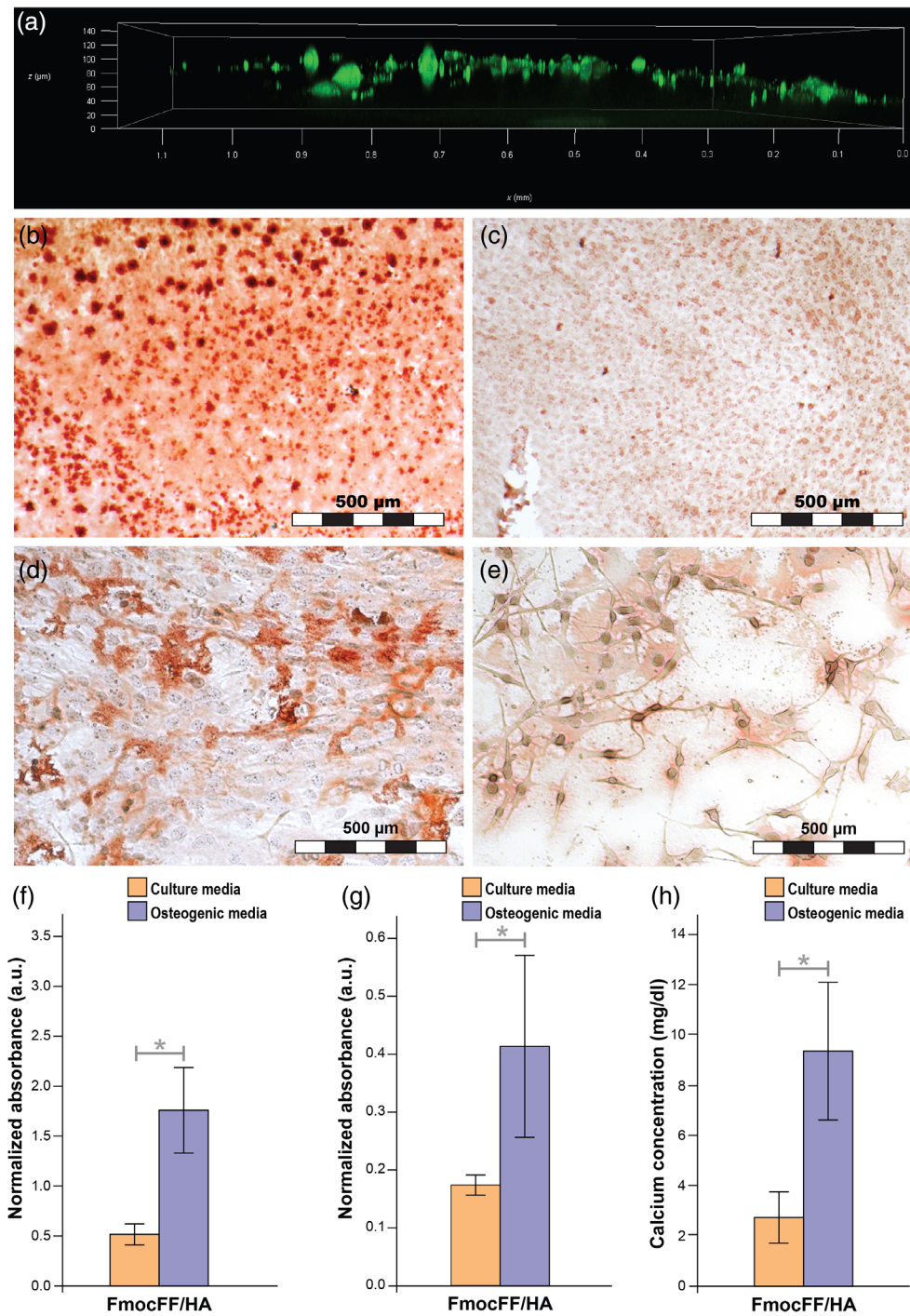


FIGURE 3 Migration and osteogenic differentiation of MC3T3-E1 preosteoblasts on the hydrogel (a) migration of MC3T3-E1 preosteoblasts 1 day after seeding using confocal microscopy. (b) Optic microscope images of MC3T3-E1 preosteoblasts stained with Alizarin red 14 days after seeding on FmocFF/hyaluronic acid (HA) hydrogel with osteogenic media. (c) Optic microscope images of MC3T3-E1 preosteoblasts stained with Alizarin red 14 days after seeding on FmocFF/HA hydrogel with culture media. (d) Optic microscope images of MC3T3-E1 preosteoblasts stained with Alizarin red 14 days after seeding on the plate with osteogenic media. (e) Optic microscope images of MC3T3-E1 preosteoblasts stained with Alizarin red 14 days after seeding on the plate with culture media. (f) Normalized Alizarin red staining absorbance values 14 days after MC3T3-E1 osteogenic differentiation with and without osteogenic media. (g) Normalized alkaline phosphatase activity of MC3T3-E1 preosteoblasts 14 days after seeding with and without osteogenic differentiation. (h) Quantification of calcium content in the supernatant of the FmocFF/HA hydrogel 14 days after seeding with and without osteogenic media. Data analysed using a two-tailed Student's *t*-test. **p* < .05, ***p* < .01

3.2 | In vitro assessment of the biocompatibility of the hydrogel and its effect on osteodifferentiation of MC3T3-E1 preosteoblasts

We assessed the migration and osteoinductive potential of the FmocFF/HA composite hydrogel by using it as a substrate for the

growth of MC3T3-E1 preosteoblasts. Cell migration could be observed already 1 day post-seeding using confocal microscopy (Figure 3a). Moreover, the hydrogel efficiently induced the differentiation and mineralization of MC3T3-E1 preosteoblasts. Matrix mineralization was quantified by Alizarin red staining calculated 14 days after cell seeding, with and without osteogenic differentiation. Staining was

FIGURE 2 Rheological and Fourier-transform infrared (FTIR) analyses of FmocFF/hyaluronic acid (HA) composite hydrogel. (a) FTIR spectra of FmocFF/HA, FmocFF and HA. (b) In situ time-sweep oscillation measurements of the FmocFF, HA, and the composite FmocFF/HA hydrogel. (c) Viscosity versus shear rate of the FmocFF/HA composite hydrogel. (d) Time sweep when alternate step strain switched from 0.1% to 100%. (e and f) Digital images demonstrating the self-healing properties of separate layers of the composite hydrogel. (g) Inverted test tube showing the self-healing property of the hydrogel after mechanical breaking

normalized to the number of cells. Figure 3b,c shows that when seeded on the FmocFF/HA hydrogel, the intensity of Alizarin red staining was higher for cells grown in osteogenic media (Figure 3b) compared with cells treated grown in culture media (Figure 3c). The staining intensity is also higher compared with cell seeded on the plate with and without differentiation media (Figure 3d,e). As shown in Figure 3f, the quantified intensity of Alizarin red staining was higher in differentiated cells than in cells without differentiation media ($p = .0126$). This result was confirmed by the normalized quantification of ALP activity the cells grown on the hydrogel and of calcium content in the supernatant of the hydrogel (Figure 3g). Fourteen days after osteogenic differentiation, an increase in ALP activity was observed compared with cells seeded on the hydrogels and treated with culture media ($p = .0143$, Figure 3g). In addition, higher amounts of calcium deposits were found in the supernatant of the hydrogel when compared with undifferentiated cells grown for 14 days in regular culture media ($p = .0211$, Figure 3h) or osteogenic media ($p = .0328$). Finally, higher calcium deposition was observed in the supernatant of the hydrogel with osteoinductive agents than without osteogenic media ($p = .0177$, Figure 3h).

3.3 | Examining the biocompatibility of the FmocFF/HA hydrogel in vivo using a rat subcutaneous model

Following FmocFF/HA hydrogel characterization and in vitro assessment, its biocompatibility was assessed in a rat subcutaneous model. FmocFF/HA hydrogel, soaked with bone marrow harvested from the femur of homologous individuals, was implanted subcutaneously in five 8-week-old Sprague-Dawley rats. After 8 weeks, the implanted material was harvested, decalcified in EDTA, stained with H&E and visualized microscopically. The hydrogel has led to the formation of adipocytes with no signs of inflammation (Figure S3).

3.4 | In vivo assessment of bone regeneration in critical-sized defects with FmocFF/HA composite hydrogel

3.4.1 | Micro-CT analysis of critical-sized bone defects in vivo

In order to assess the potential of the FmocFF/HA hydrogel to serve as a scaffold for bone regeneration, we investigated its ability to induce bone formation in a rat calvarial critical-sized defect model. The hydrogel's stiffness (G') was confirmed and found to be 48,780 Pa. A critical-size defect 5 mm in diameter was created in the right parietal bone of each rat. Each defect was filled with either FmocFF/HA hydrogel, small particles of deproteinized BBM, FmocFF/Alg hydrogel (positive controls) or left unfilled (a negative control). All animals survived the implantation surgery and exhibited uneventful postoperative healing. Eight weeks after implantation, hydrogel

remnants were not observed in the treated sites. Newly formed bone was observed in all groups (Figure 4a). Coronal cross-sections of the defects in the four groups revealed that unfilled defects contained newly formed bone only at the defect margins, while, in the defects filled with FmocFF/HA, BBM, or FmocFF/Alg, the newly formed bone bridged the defect. Notably, the newly formed mineralized tissue in the FmocFF/HA-filled defect was indistinguishable from the surrounding native bone. In the FmocFF/Alg treatment, the newly formed bone was homologous to the native bone; however, its thickness decreased towards the centre of the defect with some unfilled areas. In the BBM-filled defects, bony islands could be observed in direct contact with the graft particles and particularly adjacent to the dural side. Residual BBM particles were observed in the defect area, with some particles extending outside of the defect area close to the periosteal side.

The top view colour map demonstrates a decrease in bone thickness from the defect margins inward in the unfilled defect group as well as in the FmocFF/Alg hydrogel group. By contrast, in the FmocFF/HA hydrogel group, the thickness of the newly formed bone was homogeneous throughout the defect, with a similar or even higher thickness than of the untreated control side. The thickness of the newly formed bone in the BBM-filled defects was relatively low and inconsistent across the region (Figure 4a).

The mean restored bone volume was calculated and compared between the four groups (Figure 4b). In the FmocFF/HA hydrogel group, the restored bone volume was $92.95 \pm 32.77\%$. Significantly lower values of $37.89 \pm 21.27\%$ ($p = .0256$), $41.20 \pm 30.46\%$ ($p = .0355$) and $59.06 \pm 27.70\%$ were observed in the unfilled defect, BBM and FmocFF/Alg groups, respectively (Figure 4b). The majority of the defect ($72.52 \pm 34.99\%$) in the BBM group was composed of residual graft particles. To investigate further, the restored bone volume in three different regions of the defect, namely, outer, middle and inner areas, was compared (Figure 4c). In the unfilled defects, there was a trend to a decrease in the mean bone volume when moving from the edges of the defect towards the inner section, with values of $51.11 \pm 23.59\%$ at the periphery but $32.13 \pm 19.94\%$ in the mid-section, and $28.15 \pm 17.06\%$ in the inner. A similar trend was observed in the BBM group, where the mean bone volumes decreased from $51.95 \pm 24.77\%$ at the edge, through $38.77 \pm 31.71\%$ in the mid-section, to $31.41 \pm 30.33\%$, in the inner, and in the FmocFF/Alg hydrogel where the bone volumes decreased from $69.97 \pm 24.06\%$ at the edge, through $58.22 \pm 24.20\%$ in the mid-section, to $49 \pm 35.60\%$ in the inner. Notably, in the FmocFF/HA hydrogel treatments, bone volumes were seen throughout the repaired defect, with similar values across the three regions: $94.23 \pm 19.55\%$, $93.16 \pm 31.79\%$ and $91.64 \pm 39.37\%$, in the outer, middle and inner regions, respectively. The differences in mean bone volume between the FmocFF/HA and the unfilled defect groups were statistically significant in all three regions ($p = .0489$, $p = .0257$ and $p = .0298$ for the outer, middle and inner regions, respectively). A statistically significant difference in mean bone volume was observed between the FmocFF/HA and the BBM groups in the middle and inner regions ($p = .0463$ and $p = .0390$, respectively).

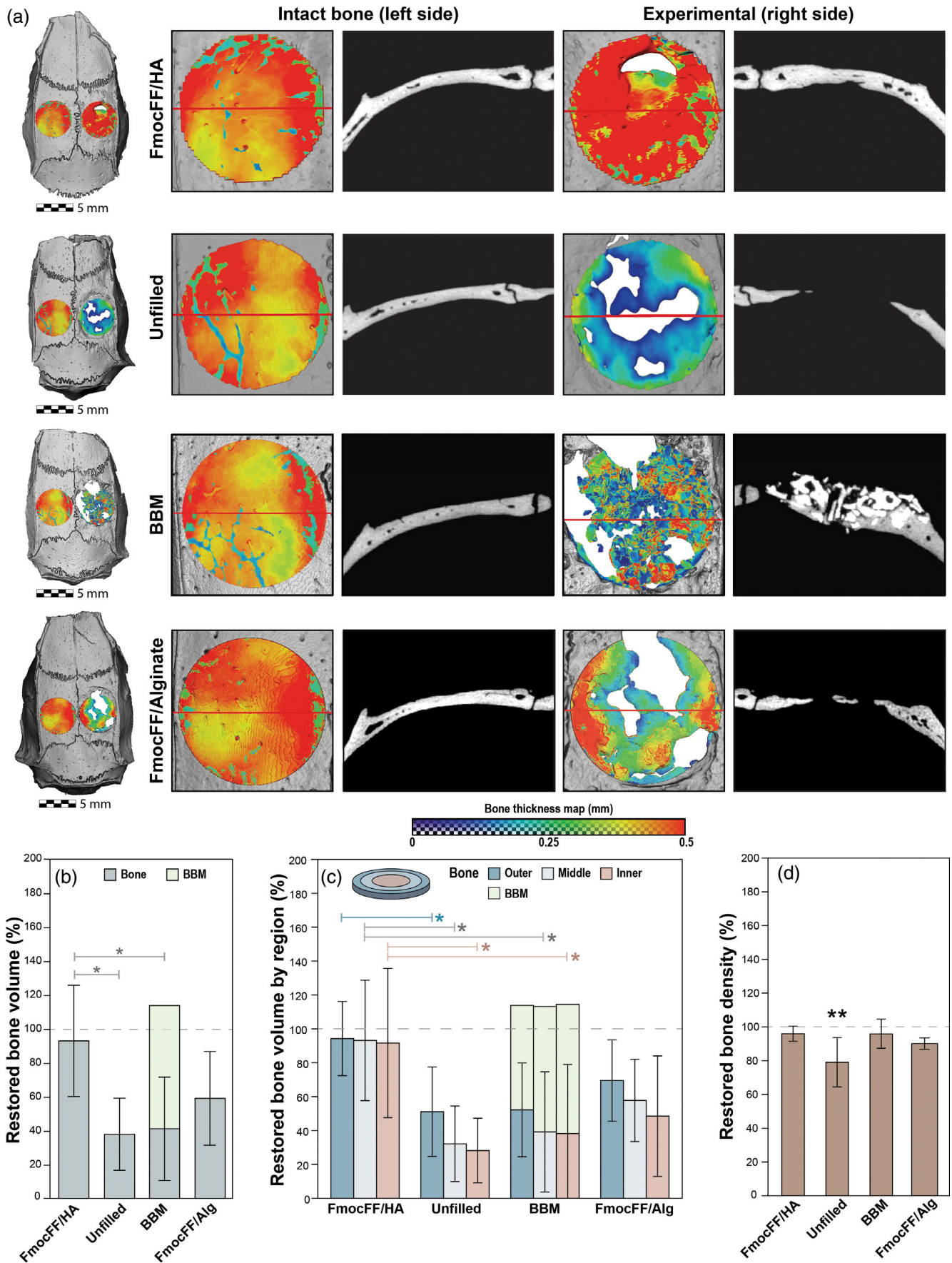


FIGURE 4 Legend on next page.

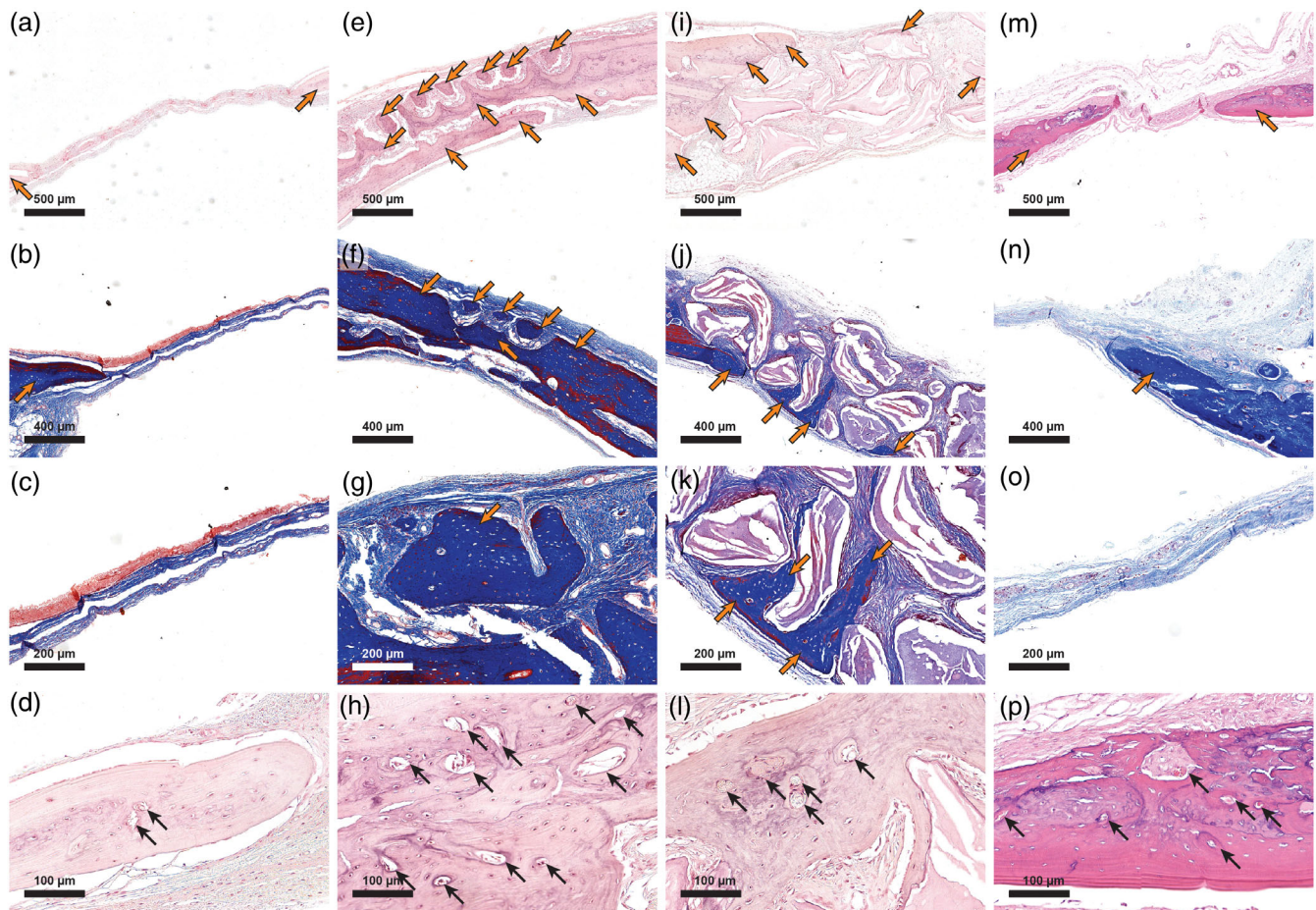


FIGURE 5 Histologic sections of the bone defect repair 8 weeks post-surgery. (a) haematoxylin and eosin (H&E) staining of the unfilled defect. Bone emerging from the defect margins is seen on both sides (orange arrows). (b) Masson's trichrome staining of the unfilled defect. Bone emerging from the defect margin is seen on the left (orange arrow). (c) High magnification of a Masson's trichrome staining of the unfilled defect. (d) Demonstration of blood vessels in the newly formed bone in an unfilled defect (black arrows). (e) H&E staining of the FmocFF/hyaluronic acid (HA) hydrogel-filled defect shows bone emerging from the defect margins as well as bone islands (orange arrows). (f) Masson's trichrome staining of the FmocFF/HA hydrogel-filled defect shows bone islands (orange arrows). (g) High magnification of a Masson's trichrome staining of the FmocFF/HA hydrogel-filled defect showing a bone island containing osteocytes (orange arrow). (h) Demonstration of blood vessels in the newly formed bone in a defect filled with FmocFF/HA hydrogel (black arrows). (i) H&E staining of the defect filled with bovine bone mineral (BBM). Bone emerging from the defect margin is seen on the left (orange arrows). (j) Masson's trichrome staining of the defect filled with BBM showing new bone surrounding the BBM particles (orange arrows). (k) High magnification of a Masson's trichrome staining of the defect filled with BBM (orange arrows showing new bone formation). (l) Blood vessels formed in the new bone surrounding the BBM particles (black arrows). (m) H&E staining of FmocFF/Alg-filled defect. Bone emerging from the defect margins is seen on both sides (orange arrows). (n) Masson's trichrome staining of FmocFF/Alg-filled defect. Bone emerging from the defect margin is seen on the right (orange arrow). (o) High magnification of a Masson's trichrome staining of FmocFF/Alg-filled defect. (p) Demonstration of blood vessels in the newly formed bone in FmocFF/Alg-filled defect (black arrows)

FIGURE 4 In vivo assessment of the FmocFF/hyaluronic acid (HA) composite hydrogel in critical-sized bone defects using micro-computed tomography (micro-CT) at 8 weeks. (a) Representative microCT reconstructions of rat calvarial defects in the four groups (FmocFF/HA, unfilled, bovine bone mineral [BBM] and FmocFF/Alg). A colour map representing the thickness of the repaired defect (right side of the calvaria) compared to the corresponding untreated control (left side of calvaria) was made on top view images of the calvarias. Red colour indicates a high thickness value, while blue indicates low thickness values. A coronal section of each defect was made to compare the quality of defect fill in the experimental and untreated control group. (b) Mean restored bone volume in the four groups. The dark green part of the columns represents new bone and the light green represents residual graft particles. (c) Mean restored bone volume divided into three areas with equal volumes, namely inner, middle, and outer. The light green part of the columns in the BBM group represents residual graft particles. (d) Mean restored bone mineral density in the four groups relative to the untreated control. Data analysed using two-way analysis of variance (ANOVA) with Bonferroni post hoc test and one-way ANOVA with Tukey's post-test, * $p < .05$

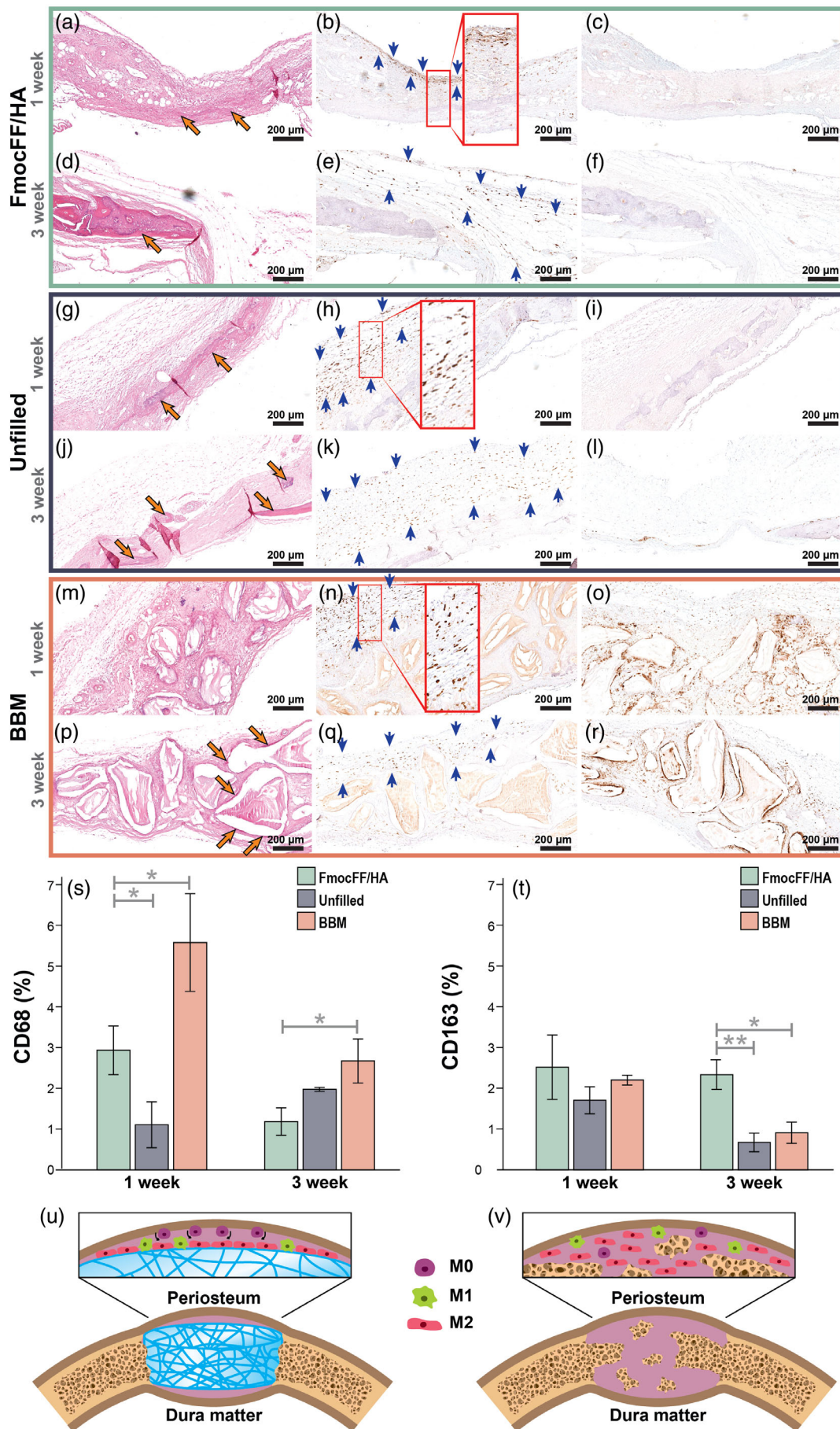


FIGURE 6 Legend on next page.

Figure 4d demonstrates the newly formed bone density, calculated relative to the intact contra-lateral bone. In both the FmocFF/HA and the BBM groups, the new bone density was almost similar to that of the original bone, with values of $95.94 \pm 3.86\%$ ($p = .7217$) and $95.98 \pm 7.72\%$ ($p > .9999$), respectively. A lower bone density value of $79.03 \pm 13.05\%$ was observed in the unfilled defect group, which was significantly different ($p = .0083$) from the original bone.

3.4.2 | Histological evaluation

In order to complement the micro-CT evaluation, we performed histological analysis. After 8 weeks, the unfilled defects contained newly mineralized tissue, including new blood vessels, extending from the defect margins (Figure 5a-d), while the central region of the defects was filled with fibrous connective tissue comprising fibroblasts and blood vessels. By contrast, the FmocFF/HA hydrogel-filled defects contained higher amounts of new bone formation that not only originated from the defect margins but was also evident in the central portion of the defects (Figure 5e). At higher magnification, islands of newly formed bone that do not start at the margins of the defect were evident (Figure 5f,g). Both osteocytes and new blood vessels entrapped in these bone islands indicated the viability of the newly formed bone (Figure 5g,h). In the defects filled with BBM, several particles surrounded by newly formed bone were evident, while most of the particles were surrounded by connective tissue (Figure 5i-k). The newly formed bone was mostly continuous with the defect margins; however, the bone formed around the BBM particles included entrapped osteocytes and blood vessels, indicating the new bone's viability (Figure 5l). In the FmocFF/Alg hydrogel-filled defect, similar to the unfilled defects, new bone arising from the defect edges with new blood vessels could be observed (Figure 5m-p).

3.4.3 | Osteoimmunomodulation of the FmocFF/HA hydrogel

Having demonstrated that the FmocFF/HA hydrogel resulted in complete restoration of the calvarial critical-sized defect, we sought to determine whether macrophage polarization may play a role in this process compared with unfilled defects and to defects filled with BBM. CD68 and CD163 immunohistochemical labelling was used to visualize M1 (pro-inflammatory) and M2 (pro-regenerative) macrophages, respectively, in the calvarial defect (Tournier et al., 2021). Baseline levels of M2 and M1 macrophages at 1 and 3 weeks after implantation were observed in the intact left parietal side (Figure S4). One-week post-implantation, a low amount of M2 and M1 macrophages can be observed under the periosteum (Figure S4a,b, respectively). At 3 weeks after implantation, slightly higher amounts of M2 and M1 macrophages can be detected (Figure S4c,d, respectively). In the FmocFF/HA hydrogel group, 1 week after implantation, a beginning of bone formation could be seen in the middle of the defect (Figure 6a). Elongated M2 macrophages were detected at the hydrogel–periosteum interface (Figure 6b), while M1 macrophages were hard to discern (Figure 6c). At 3 weeks of regeneration, bigger bone islands could be observed (Figure 6d). M2 macrophages were observed above and under the newly formed bone adjacent to the periosteum and the dura mater, respectively, and between the bone islands throughout the regenerating tissue (Figure 6e). At this time point as well, M1 macrophages were hard to discern (Figure 6f). In the unfilled defects, M2 macrophages could be observed both at 1 and 3 weeks, while M1 population was hardly observed (Figure 6g-l). In the BBM group 1 week after implantation, both M1 and M2 macrophages could be observed. The M2 population was located under the periosteum on top of the BBM particles, while the M1 population was seen also under the periosteum but mainly surrounding the BBM

FIGURE 6 Immunomodulation of the FmocFF/hyaluronic acid (HA) hydrogel 1 and 3 weeks after implantation (a) haematoxylin and eosin (H&E) staining of the FmocFF/HA-filled defect 1 week after implantation showing initial bone formation (orange arrows). (b) Immunohistochemical staining for CD163 1 week after FmocFF/HA hydrogel implantation. Brown staining indicating M2 macrophages lining at the hydrogel–periosteum interface (blue arrows). (c) Immunohistochemical staining for CD68 (M1 macrophages, brown staining) 1 week after FmocFF/HA hydrogel implantation. (d) H&E staining of the FmocFF/HA-filled defect 3 weeks after implantation showing new bone formation (orange arrows). (e) Immunohistochemical staining for CD163 (M2 macrophages) 3 weeks after FmocFF/HA hydrogel implantation showing brown staining of cells along the regenerating tissue (blue arrows). (f) Immunohistochemical staining for CD68 (M1 macrophages) 3 weeks after FmocFF/HA hydrogel implantation. (g) H&E staining of the unfilled defect 1 week after surgery (orange arrows showing new bone). (h) Immunohistochemical staining for CD163 (M2 macrophages, brown staining) in the unfilled defect 1 week after surgery (blue arrows showing M2 macrophages). (i) Immunohistochemical staining for CD68 (M1 macrophages, brown staining) in the unfilled defect 1 week after surgery. (j) H&E staining of the unfilled defect 3 weeks after surgery showing initial bone formation (orange arrows). (k) Immunohistochemical staining for CD163 (M2 macrophages) in the unfilled defect 3 weeks after surgery (blue arrows). (l) Immunohistochemical staining for CD68 (M1 macrophages) in the unfilled defect 3 weeks after surgery. (m) H&E staining of the bovine bone mineral (BBM)-filled defect 1 week after surgery. (n) Immunohistochemical staining for CD163 (blue arrows) 1 week after surgery. (o) Immunohistochemical staining for CD68 (M1 macrophages, brown staining) of the BBM-filled defect 1 week after implantation. (p) H&E staining of the BBM-filled defect 3 weeks after implantation (orange arrows showing new bone). (q) Immunohistochemical staining for CD163 (M2 macrophages) of the BBM-filled defect 3 weeks after implantation (blue arrows). (r) Immunohistochemical staining for CD68 (M1 macrophages) of the BBM-filled defect 3 weeks after implantation. (s) Quantification of CD68 positive macrophages at 1 week and 3 weeks and comparison between the three groups (FmocFF/HA, BBM and unfilled defects.) (t) Quantification of CD163 positive cells at 1 and 3 weeks and comparison between the three groups (FmocFF/HA, BBM and unfilled defects.) (u and v) Schematic illustration of the immunomodulation induced by the hydrogel 1 (u) and 3 (v) weeks after implantation (purple cells = resident macrophages, M0 macrophages; green cells = M1 macrophages; red cells = M2 macrophages)

particles. After 3 weeks, both M1 and M2 macrophages were seen between the BBM particles (Figure 6m-r). Interestingly, quantification of M1 and M2 macrophages shows that in the FmocFF/HA hydrogel group, at 1 week, M1 was greater than M2, while at 3 weeks, M2 was greater than M1 (Figure 6s,t). A reduction in M1 was observed from 1 to 3 weeks. In the unfilled defect, M2 was greater than M1 at 1 week; however, at 3 weeks, M1 was greater than M2. In the BBM group, M1 was greater than M2 at both time points. Notably, after 3 weeks, the FmocFF/HA hydrogel group demonstrated low presence of M1 cells and the highest presence of M2 cell compared with BBM or unfilled defect groups ($p = .0298$ and $p = .0526$ for M1, respectively, and $p = .0181$ and $p = .0025$ for M2, respectively). These results may suggest the effect of the FmocFF/HA hydrogel on macrophage polarization into M2 macrophages, which may play a key role in bone regeneration in vivo (Figure 6u,v).

4 | DISCUSSION

A key challenge in bone regeneration is to fabricate a biocompatible, biodegradable, rigid scaffold that can induce an immunomodulatory response of the surrounding tissues to activate a regeneration path of angiogenesis and osteogenesis and restore the architecture of natural bone (Holzwarth & Ma, 2011). The aim of the present study was to develop a composite FmocFF/HA hydrogel as a biomaterial to treat critical-sized bone defects. The results demonstrate that the FmocFF/HA hydrogel mimics the native ECM and provides a temporary biodegradable 3D matrix to facilitate osteogenic differentiation and bone tissue formation in vitro. Moreover, in vivo, the hydrogel was well integrated with the surrounding bone tissue and allowed a complete restoration of calvarial defects.

Incorporating FmocFF, a short aromatic self-assembling peptide, into a HA matrix produces a biomimetic structure in which FmocFF resembles the collagen fibrils and the HA resembles the glycosaminoglycans, which are the two main components of native ECM (Aviv et al., 2018). A similar interaction between HA and a tripeptide hydrogelator, Fmoc-FFY, by localized enzyme-assisted self-assembly approach has formed hydrogel coatings in various thicknesses determined by the concentration of the HA (Rodon Fores et al., 2021).

The entangled dense nanofibrous architecture demonstrated by electron microscopy is of utmost importance in ensuring good infiltration of cells, nutrients and oxygen throughout the construct and facilitating waste transport (R. Zhang & Ma, 2000; Holzwarth & Ma, 2011). Biomimetic nanofibrous scaffolds have been shown to enhance the attachment of MC3T3-E1 osteoblasts in vitro and the osteogenic potential of mouse calvarial osteoblasts in vivo, compared with solid-wall scaffolds (Woo et al., 2003, 2007). It is assumed that it is the selective enhancement of adsorption of proteins such as fibronectin, vitronectin and laminin by nanofibrous scaffolds that allow a large number of cells to bind tightly to the matrix (Woo et al., 2003). Mineralization by MC3T3-E1 preosteoblasts in vitro is facilitated by the formation of matrix vesicles surrounding the osteoblasts and osteocytes followed by calcification of the organic matrix (Sudo et al., 1983). This

mineralization process is similar to intramembranous osteogenesis in vivo, such as in the calvaria, the in vivo model used in the present study.

Another factor determining the ability of a scaffold to promote bone regeneration is stiffness. Stiff substrates not only induce greater spreading of cells (Pelham & Wang, 1997), but this parameter also determines DNA methylation (Zhao et al., 2021) and secretory profiles of stem cells (Engler et al., 2006; Alakpa et al., 2016), which further directs their phenotype (Seib et al., 2009). Hydrogels exhibiting a storage modulus of >30 kPa were found to promote an osteoblastic phenotype in stem cells (Engler et al., 2006; Pek et al., 2010; Alakpa et al., 2016), while scaffolds with lower storage modulus values like 1 and 13 Pa rather promoted neuronal and chondrogenic differentiation respectively (Alakpa et al., 2016). Recently, we have shown that the combinations of FmocFF and HA can be varied to obtain hydrogels with customized mechanical properties (Aviv et al., 2018; Nadernezhad et al., 2020). The stiffness of the hydrogel was influenced by the ratio between HA and the FmocFF. Increasing the hydrogel's peptide ratio increased the stiffness to a maximal value of 25 kPa at a FmocFF/HA 3:1 ratio (Aviv et al., 2018). In the current study, FmocFF/HA was fabricated at a ratio of 3:1; however, the peptide concentration used was higher, which may explain the higher storage modulus of 46 kPa (Figure 2). The storage modulus value indicates a stiffness optimized for osteogenic differentiation (Alakpa et al., 2016). Furthermore, the high stiffness of the hydrogel allows it to hold a customized shape. Also, due to the injectability, the hydrogel can adapt to irregular-shaped bone defects, making it useful for minimally invasive surgical procedures.

Alizarin red staining, ALP activity and calcium quantification analyses performed after 14 days of cell culture indicated the osteopromotion of this organic FmocFF/HA hydrogel (Figure 3). These results are in accordance with our previously reported FmocFF/Alg composite hydrogel (Ghosh et al., 2019), FmocFF/Sulphated polysaccharide (Halperin-Sternfeld et al., 2022) and additional periosteal ECM hydrogel (Qiu et al., 2020). All induced in vitro mineralization without containing inorganic particles. We suggest that the hydrogel serves as a 3D matrix that facilitates cell attachment, proliferation, osteogenic differentiation and mineralization. Moreover, in vivo, the hydrogel was also shown to be osteoinductive in the rat critical-sized bone defect model used in this study. It should be noted that the calvarial defect fill involves immune cell responses to the biomaterial, which are challenging to model in vitro.

The host immune response has now been established as the most critical factor determining the fate of a biomaterials (Brown et al., 2012; Hao et al., 2017). In particular, the macrophage response to an implanted biomaterial can orchestrate the transition from inflammatory to regenerative phenotype and guide the other inflammatory cells to complete the wound-healing process in critical-sized defects (Hao et al., 2017). Following implantation of biomaterials, during the inflammatory phase, both pro-inflammatory M1 and pro-regenerative M2 macrophages populate the wound site (Yang et al., 2018). The ratio between the two phenotypes depends on the chemical and physical properties of the biomaterials and is an

essential factor for wound healing and tissue regeneration (Yang et al., 2018). As the cell-free FmocFF/HA hydrogel scaffold induced almost complete bone formation and restored the original density of the bone in the rat critical-sized bone defect, we can surmise that its chemical and mechanical properties were responsible for the incitement and promotion of the host natural bone healing process driven by the M2 pro-regenerative macrophages. At 1 week of regeneration, the hydrogel recruits resident macrophages from the periosteum and circulating monocyte precursors to the hydrogel–periosteum interface (Figure 6g). M2 macrophages dominate along the hydrogel surface and demonstrate elongated shape, indicating their ability to reduce inflammatory cytokines expression, enhance the secretion of IL-4 and IL-13 and protect cells from M1 macrophages that induce LPS and IFN- γ (McWhorter et al., 2013). At 3 weeks of regeneration, an increase in the M2 population along the regenerating tissue indicates further recruitment of circulating monocytes from the new blood vessels created in the defect site (Figure 6g). We assume that the high M2 population recruited by the hydrogel from the periosteum and the blood vessels promotes the osteogenesis process in the defect site to induce bone regeneration. This regeneration process induced by M2 macrophages is initiated by the secretion of anti-inflammatory factors, recruitment of progenitor cells and the production of growth factors that regulate their differentiation and angiogenesis (Mosser & Edwards, 2008; Murray & Wynn, 2011). A previous study has elucidated the regenerative potential of the periosteum (Duchamp de Lageneste et al., 2018). Although it has been primarily assigned to resident mesenchymal progenitor cells (Duchamp de Lageneste et al., 2018), the involvement of resident macrophages in this process is evident in the present study. M2 macrophages are pro-regenerative and can affect the residing mesenchymal cells for osteogenesis (Löffler et al., 2019). Therefore, it can be surmised that the presence of the periosteum is necessary for the hydrogel induction of osteogenesis. The formation of adipocytes, which derive from mesenchymal stem cells in the subcutaneous model, may also be a source of multipotent cells that may later differentiate into osteogenic cells (Zuk et al., 2001).

The effect of the FmocFF/HA hydrogel on bone formation was compared with unfilled defects serving as a negative control and defects treated with BBM, a commercial xenograft known for its osteoconductive properties, and the previously reported FmocFF/Alg hydrogel as positive controls. The FmocFF/HA hydrogel proved superior to all the other interventions in bone repair. Although new bone formation and neovascularization were observed 8 weeks after the surgical procedure in all groups, the volume of the restored bone in the FmocFF/HA hydrogel repaired defects was more than twice that in the controls. Similarly, although bone formation in the repair of all the experimental groups followed the well-documented pattern from the defect margins inwards, histological analysis revealed that the FmocFF/HA hydrogel repair also included bony islets in the centre of the defect that were separated from the margins. This observation was confirmed by the micro-CT analysis of the hydrogel-filled defects, where the volume of restored bone was essentially homogeneous across the outer, middle and inner regions of the defect (Figure 4c).

By contrast, the micro-CT analysis of unfilled-, FmocFF/Alg and BBM-filled defects revealed that the bone volume was higher around the outer edge and decreased towards the inner regions of the defect (Figure 4c). Notably, the generation of bony islets most probably originates from the dura mater and the periosteum, areas known for their osteogenic potential (Sohn et al., 2010). Their study of spontaneous bone healing in rabbit cranial defects described the formation of bone islands in the centre of the defects in addition to the bone formed from the defect margins (Sohn et al., 2010). Notably, in the present study, this finding was only observed in the FmocFF/HA hydrogel group, despite the presence of dura mater and periosteum in all four groups, and may therefore be attributed to the ability of the FmocFF/HA hydrogel to sustain the defect site over time and direct immunomodulation towards a regenerative process.

There was no statistically significant difference in the percentage of restored bone volume between unfilled defects and defects filled with BBM. We speculate that this lack of superiority was due to the micromovement of the BBM particles, both inside and outside the defect area, as observed in the cross-sectional micro-CT images. Such a micromovement may be attributed to the lack of bonding of the BBM particles. Indeed, it has been previously reported that angiogenesis and subsequent bone regeneration are highly affected by the stability of the grafted material (Boerckel et al., 2011). Another possible explanation could be the inability of BBM to stimulate the periosteum and blood clot cells to form bone (Kübler & Urist, 1990). Although restricted to the margins, it should be noted that the percentages of the restored bone volumes in the unfilled and BBM-filled defects in the present study are relatively higher (~40%) than previously described. Park et al. (2009) reported that after 12 weeks, the percentage of new bone volume in unfilled and BBM-filled rat critical-sized bone defects were $6.4 \pm 4.8\%$ and $8.2 \pm 3.9\%$, respectively. This difference may result from the larger defect size of 8 mm used in their study.

The newly formed bone in the FmocFF/HA hydrogel group was well integrated and indistinguishable from native bone, meaning that the hydrogel fully restored the original thickness of the calvaria and the newly formed bone density was similar to that of the original bone. By contrast, the newly formed bone extending from the defect margins in the unfilled defect group could not bridge the defect. Instead, its height gradually decreased from the defect margins inward. These findings emphasize the necessity of a scaffold in significant bone defects. Whereas the innate healing capacity originates at the defect margins (Sohn et al., 2010), the main contribution of the scaffold is to promote bone formation in the central parts of the defect, where the bone formation process is slow and the blood supply is limited. The new vital bone, which contains osteocytes and blood vessels as observed in the histological sections, may then enhance the contribution of the scaffold in the FmocFF/HA group.

The superior performance of FmocFF/HA over FmocFF/Alg hydrogel may be attributed to the interaction of high molecular weight HA with the CD44 receptor that promotes the production of anti-inflammatory cytokines like IL10 and inhibits the pro-inflammatory TLR signalling, as previously suggested (Ruppert

et al., 2014). Furthermore, the interaction of the high molecular weight HA with CD44 receptor leads to the infiltration of circulating osteoprogenitors and innate immune cells that synthesize bone tissue and contributes to the restoration of bone tissue architecture (Turley et al., 2002).

The limitation of the study is the discrepancy observed between the in vitro results and the significant bone regeneration found in the calvarial defects. In vitro, a cell line of preosteoblasts was used. This may hinder the entire milieu of cell interactions required for bone regeneration and angiogenesis. In vivo, however, the hydrogel interaction with the periosteum and the ability of high molecular weight HA to interact with CD44 receptors towards osteogenesis may explain the restoration of the calvarial defect.

5 | CONCLUSION

Overall, the in vitro and in vivo results demonstrate an osteo-regenerative effect of the FmocFF/HA hydrogel. Incorporating the self-assembling peptide, FmocFF, into the HA matrix resulted in forming a stiff fibrous hydrogel with a storage modulus value that has been reported as beneficial for promoting bone regeneration without the need for inorganic bone ceramics for reinforcement. The resemblance of the hydrogel to the native bone ECM supported MC3T3-E1 preosteoblast osteodifferentiation. In vivo, 8 weeks after implantation into a rat calvarial critical-sized bone defect, the hydrogel induced bone formation of approximately 95% of the original volume, two-fold higher than seen either in unfilled defects or in defects filled with a xenogenic bone graft. The scaffold not only induced bone deposition from the defect margins but also created bony islets in the central part of the defect. These two patterns of bone formation resulted in the complete restoration of the original thickness of the calvaria and its original bone density. It can be surmised that the hydrogel served as a 3D matrix that maintained the space over time and was then gradually degraded while promoting the host's natural bone healing process by modulating the local immune environment in favour of angiogenesis, osteogenesis and the osteointegration of the implanted hydrogel. Finally, its simple production, relatively low cost and ease of handling and delivery, both as an injectable hydrogel and as a custom-made construct, demonstrate its potential for use in various clinical applications in bone regenerative medicine.

AUTHOR CONTRIBUTIONS

Michal Halperin-Sternfeld, Moumita Ghosh, Dana Rachmiel, Raha Kannan, Itzhak Grinberg, M.A., Itzhak Binderman and Lihi Adler-Abramovich conceived and designed the experiments. Michal Halperin-Sternfeld, Moumita Ghosh, Ariel Pokhojaev, Moshe Asher, Moran Aviv, Raha Kannan, Itzhak Binderman and Lihi Adler-Abramovich analysed the data. Michal Halperin-Sternfeld wrote the original draft of the paper. Raha Kannan, Peter X. Ma, Itzhak Binderman, Rachel Sarig and Lihi Adler-Abramovich reviewed and edited the paper. Michal Halperin-Sternfeld, Ariel Pokhojaev, Moumita Ghosh, Dana Rachmiel, Raha Kannan, Itzhak Grinberg, Moshe Asher, Moran

Aviv, Peter X. Ma, Itzhak Binderman, Rachel Sarig and Lihi Adler-Abramovich discussed the results and commented on the manuscript.

ACKNOWLEDGEMENTS

This project received funding from the European Research Council (ERC) under the European Union's Horizon 2020 research and innovation programme (grant agreement no. 948102) (L.A.-A.), the Israel Science Foundation (grant no. 1732/17) (L.A.-A.) and the Ministry of Science, Technology & Space, Israel (L. A.-A.). The authors acknowledge a Clore scholarship (M.H.-S), BSF (grant no. 2018102) (M.H.-S), GRTF travel grant (M.H.-S) for support. The authors acknowledge the Chaoul Center for Nanoscale Systems of Tel Aviv University for the use of instruments and staff assistance and Yankel Gabet for assistance with micro-CT scans. Finally, the authors would like to acknowledge the Adler-Abramovich and Sarig research groups for fruitful discussions.

CONFLICT OF INTEREST

The authors declare that there is no conflict of interest.

DATA AVAILABILITY STATEMENT

The data that support the findings of this study are available from the corresponding author upon reasonable request.

ORCID

Michal Halperin-Sternfeld  <https://orcid.org/0000-0001-9242-0616>

Itzhak Binderman  <https://orcid.org/0000-0002-7352-0352>

Rachel Sarig  <https://orcid.org/0000-0002-9323-5014>

Lihi Adler-Abramovich  <https://orcid.org/0000-0003-3433-0625>

REFERENCES

- Adams, D. J., Butler, M. F., Frith, W. J., Kirkland, M., Mullen, L., & Sanderson, P. (2009). A new method for maintaining homogeneity during liquid-hydrogel transitions using low molecular weight hydrogelators. *Soft Matter*, 5, 1856–1862.
- Adams, D. J., Mullen, L. M., Berta, M., Chen, L., & Frith, W. J. (2010). Relationship between molecular structure, gelation behaviour and gel properties of Fmoc-dipeptides. *Soft Matter*, 6, 1971–1980.
- Alakpa, E. V., Jayawarna, V., Lampel, A., Burgess, K. V., West, C. C., Bakker, S. C. J., Roy, S., Javid, N., Fleming, S., Lamprou, D. A., Yang, J., Miller, A., Urquhart, A. J., Frederix, P. W. J. M., Hunt, N. T., Péault, B., Ulijn, R. V., & Dalby, M. J. (2016). Tunable supramolecular hydrogels for selection of lineage-guiding metabolites in stem cell cultures. *Chem*, 1, 298–319.
- Aviv, M., Halperin-Sternfeld, M., Grigoriants, I., Buzhansky, L., Mironi-Harpaz, I., Seliktar, D., Einav, S., Nevo, Z., & Adler-Abramovich, L. (2018). Improving the mechanical rigidity of hyaluronic acid by integration of a supramolecular peptide matrix. *ACS Applied Materials & Interfaces*, 10, 41883–41891.
- Bai, X., Gao, M., Syed, S., Zhuang, J., Xu, X., & Zhang, X. Q. (2018). Bioactive hydrogels for bone regeneration. *Bioactive Materials*, 3, 401–417.
- Beniash, E., Hartgerink, J. D., Storrer, H., Stendahl, J. C., & Stupp, S. I. (2005). Self-assembling peptide amphiphile nanofiber matrices for cell entrapment. *Acta Biomaterialia*, 1, 387–397.
- Boerckel, J. D., Uhrig, B. A., Willett, N. J., Huebsch, N., & Guldberg, R. E. (2011). Mechanical regulation of vascular growth and tissue regeneration in vivo. *Proceedings of the National Academy of Sciences of the United States of America*, 108, E674–E680.

- Brito, A., Abul-Haija, Y. M., da Costa, D. S., Novoa-Carballal, R., Reis, R. L., Ulijn, R. V., Pires, R. A., & Pashkuleva, I. (2019). Minimalistic supramolecular proteoglycan mimics by co-assembly of aromatic peptide and carbohydrate amphiphiles. *Chemical Science*, *10*, 2385–2390.
- Brown, B. N., Ratner, B. D., Goodman, S. B., Amar, S., & Badylak, S. F. (2012). Macrophage polarization: An opportunity for improved outcomes in biomaterials and regenerative medicine. *Biomaterials*, *33*, 3792–3802.
- Celik, E., Bayram, C., Akcapinar, R., Turk, M., & Denkbaz, E. B. (2016). The effect of calcium chloride concentration on alginate/Fmoc-diphenylalanine hydrogel networks. *Materials Science & Engineering. C, Materials for Biological Applications*, *66*, 221–229.
- Chakraborty, P., Roy, B., Bairi, P., & Nandi, A. K. (2012). Improved mechanical and photophysical properties of chitosan incorporated folic acid gel possessing the characteristics of dye and metal ion absorption. *Journal of Materials Chemistry*, *22*, 20291–20298.
- Cheng, W., Ding, Z., Zheng, X., Lu, Q., Kong, X., Zhou, X., Lu, G., & Kaplan, D. L. (2020). Injectable hydrogel systems with multiple biophysical and biochemical cues for bone regeneration. *Biomaterials Science*, *8*, 2537–2548.
- Chircov, C., Grumezescu, A. M., & Bejenaru, L. E. (2018). Hyaluronic acid-based scaffolds for tissue engineering. *Romanian Journal of Morphology and Embryology*, *59*, 71–76.
- Csoka, A. B., Frost, G. I., & Stern, R. (2001). The six hyaluronidase-like genes in the human and mouse genomes. *Matrix Biology*, *20*, 499–508.
- Debnath, S., Roy, S., Abul-Haija, Y. M., Frederix, P., Ramalhethe, S. M., Hirst, A. R., Javid, N., Hunt, N. T., Kelly, S. M., Angulo, J., Khimyak, Y. Z., & Ulijn, R. V. (2019). Tunable supramolecular gel properties by varying thermal history. *Chemistry*, *25*, 7881–7887.
- Deidda, G., Jonnalagadda, S. V. R., Spies, J. W., Ranella, A., Mossou, E., Forsyth, V. T., Mitchell, E. P., Bowler, M. W., Tamamis, P., & Mitraki, A. (2017). Self-assembled amyloid peptides with Arg-Gly-asp (RGD) motifs as scaffolds for tissue engineering. *ACS Biomaterials Science & Engineering*, *3*, 1404–1416.
- Derkus, B., Okesola, B. O., Barrett, D. W., D'Este, M., Chowdhury, T. T., Eglin, D., & Mata, A. (2020). Multicomponent hydrogels for the formation of vascularized bone-like constructs in vitro. *Acta Biomaterialia*, *109*, 82–94.
- Di Foggia, M., Taddei, P., Torreggiani, A., Dettin, M., & Tinti, A. (2011). Self-assembling peptides for biomedical applications: IR and Raman spectroscopies for the study of secondary structure. *Proteomics Research Journal*, *2*, 231.
- Diaferia, C., Gianolio, E., & Accardo, A. (2019). Peptide-based building blocks as structural elements for supramolecular Gd-containing MRI contrast agents. *Journal of Peptide Science*, *25*, e3157.
- Diaferia, C., Morelli, G., & Accardo, A. (2019). Fmoc-diphenylalanine as a suitable building block for the preparation of hybrid materials and their potential applications. *Journal of Materials Chemistry B*, *7*, 5142–5155.
- Diaferia, C., Netti, F., Ghosh, M., Sibillano, T., Giannini, C., Morelli, G., Adler-Abramovich, L., & Accardo, A. (2020). Bi-functional peptide-based 3D hydrogel-scaffolds. *Soft Matter*, *16*, 7006–7017.
- Dou, X. Q., & Feng, C. L. (2017). Amino acids and peptide-based supramolecular hydrogels for three-dimensional cell culture. *Advanced Materials*, *29*, 1604062.
- Draper, E. R., & Adams, D. J. (2019). Controlling the assembly and properties of low-molecular-weight hydrogelators. *Langmuir*, *35*, 6506–6521.
- Duchamp de Lageneste, O., Julien, A., Abou-Khalil, R., Frangi, G., Carvalho, C., Cagnard, N., Cordier, C., Conway, S. J., & Colnot, C. (2018). Periosteum contains skeletal stem cells with high bone regenerative potential controlled by Periostin. *Nature Communications*, *9*, 773.
- Eliezer, M., Imber, J. C., Sculean, A., Pandis, N., & Teich, S. (2019). Hyaluronic acid as adjunctive to non-surgical and surgical periodontal therapy: A systematic review and meta-analysis. *Clinical Oral Investigations*, *23*, 3423–3435.
- Engler, A. J., Sen, S., Sweeney, H. L., & Discher, D. E. (2006). Matrix elasticity directs stem cell lineage specification. *Cell*, *126*, 677–689.
- Fichman, G., & Gazit, E. (2014). Self-assembly of short peptides to form hydrogels: Design of building blocks, physical properties and technological applications. *Acta Biomaterialia*, *10*, 1671–1682.
- Franz, S., Rammelt, S., Scharnweber, D., & Simon, J. C. (2011). Immune responses to implants – A review of the implications for the design of immunomodulatory biomaterials. *Biomaterials*, *32*, 6692–6709.
- Gallo, E., Diaferia, C., Gregorio, E. D., Morelli, G., Gianolio, E., & Accardo, A. (2020). Peptide-based soft hydrogels modified with gadolinium complexes as MRI contrast agents. *Pharmaceuticals*, *13*, 19.
- Ghosh, M., Halperin-Sternfeld, M., Grigoriants, I., Lee, J., Nam, K. T., & Adler-Abramovich, L. (2017). Arginine-presenting peptide hydrogels decorated with hydroxyapatite as biomimetic scaffolds for bone regeneration. *Biomacromolecules*, *18*, 3541–3550.
- Ghosh, M., Halperin-Sternfeld, M., Grinberg, I., & Adler-Abramovich, L. (2019). Injectable alginate-peptide composite hydrogel as a scaffold for bone tissue regeneration. *Nanomaterials*, *9*, 497.
- Gong, X., Branford-White, C., Tao, L., Li, S., Quan, J., Nie, H., & Zhu, L. (2016). Preparation and characterization of a novel sodium alginate incorporated self-assembled Fmoc-FF composite hydrogel. *Materials Science & Engineering. C, Materials for Biological Applications*, *58*, 478–486.
- Halperin-Sternfeld, M., Ghosh, M., Sevostianov, R., Grigoriants, I., & Adler-Abramovich, L. (2017). Molecular co-assembly as a strategy for synergistic improvement of the mechanical properties of hydrogels. *Chemical Communications*, *53*, 9586–9589.
- Halperin-Sternfeld, M., Netanel Liberman, G., Kannan, R., Netti, F., Ma, P. X., Arad, S. M., & Adler-Abramovich, L. (2022). Thixotropic red microalgae sulfated polysaccharide-peptide composite hydrogels as scaffolds for tissue engineering. *Biomedicine*, *10*, 1388.
- Hao, S., Meng, J., Zhang, Y., Liu, J., Nie, X., Wu, F., Yang, Y., Wang, C., Gu, N., & Xu, H. (2017). Macrophage phenotypic mechanomodulation of enhancing bone regeneration by superparamagnetic scaffold upon magnetization. *Biomaterials*, *140*, 16–25.
- Hartgerink, J. D., Beniash, E., & Stupp, S. I. (2002). Peptide-amphiphile nanofibers: A versatile scaffold for the preparation of self-assembling materials. *Proceedings of the National Academy of Sciences of the United States of America*, *99*, 5133–5138.
- Hemshkhar, M., Thushara, R. M., Chandranayaka, S., Sherman, L. S., Kemparaju, K., & Girish, K. S. (2016). Emerging roles of hyaluronic acid bioscaffolds in tissue engineering and regenerative medicine. *International Journal of Biological Macromolecules*, *86*, 917–928.
- Heslop, J. A., Hammond, T. G., Santeramo, I., Tort Piella, A., Hopp, I., Zhou, J., Baty, R., Graziano, E. I., Proto Marco, B., Caron, A., Skold, P., Andrews, P. W., Baxter, M. A., Hay, D. C., Hamdam, J., Sharpe, M. E., Patel, S., Jones, D. R., Reinhardt, J., ... Park, B. K. (2015). Concise review: Workshop review: Understanding and assessing the risks of stem cell-based therapies. *Stem Cells Translational Medicine*, *4*, 389–400.
- Holzwarth, J. M., & Ma, P. X. (2011). Biomimetic nanofibrous scaffolds for bone tissue engineering. *Biomaterials*, *32*, 9622–9629.
- Huang, R., Qi, W., Feng, L., Su, R., & He, Z. (2011). Self-assembling peptide-polysaccharide hybrid hydrogel as a potential carrier for drug delivery. *Soft Matter*, *7*, 6222–6230.
- Ischakov, R., Adler-Abramovich, L., Buzhansky, L., Shekhter, T., & Gazit, E. (2013). Peptide-based hydrogel nanoparticles as effective drug delivery agents. *Bioorganic & Medicinal Chemistry*, *21*, 3517–3522.
- Jayawarna, V., Ali, M., Jowitt, T. A., Miller, A. F., Saiani, A., Gough, J. E., & Ulijn, R. V. (2006). Nanostructured hydrogels for three-dimensional cell culture through self-assembly of fluorenylmethoxycarbonyl-dipeptides. *Advanced Materials*, *18*, 611–614.
- Jayawarna, V., Richardson, S. M., Hirst, A. R., Hodson, N. W., Saiani, A., Gough, J. E., & Ulijn, R. V. (2009). Introducing chemical functionality in Fmoc-peptide gels for cell culture. *Acta Biomaterialia*, *5*, 934–943.

- Khadeja, L., Grigoriants, I., Halperin-Sternfeld, M., Yona, A., & Adler-Abramovich, L. (2019). Sonochemical functionalization of cotton and non-woven fabrics with bio-inspired self-assembled nanostructures. *Israel Journal of Chemistry*, 60, 1190–1196.
- Kisiday, J., Jin, M., Kurz, B., Hung, H., Semino, C., Zhang, S., & Grodzinsky, A. J. (2002). Self-assembling peptide hydrogel fosters chondrocyte extracellular matrix production and cell division: Implications for cartilage tissue repair. *Proceedings of the National Academy of Sciences of the United States of America*, 99, 9996–10001.
- Kobayashi, T., Chanmee, T., & Itano, N. (2020). Hyaluronan: Metabolism and function. *Biomolecules*, 10, 1525.
- Kong, J., & Yu, S. (2007). Fourier transform infrared spectroscopic analysis of protein secondary structures. *Acta Biochimica et Biophysica Sinica*, 39, 549–559.
- Kretsinger, J. K., Haines, L. A., Ozbas, B., Pochan, D. J., & Schneider, J. P. (2005). Cytocompatibility of self-assembled beta-hairpin peptide hydrogel surfaces. *Biomaterials*, 26, 5177–5186.
- Kübler, N., & Urist, M. R. (1990). Bone morphogenetic protein-mediated interaction of periosteum and diaphysis. Citric acid and other factors influencing the generation of parosteal bone. *Clinical Orthopaedics and Related Research*, 258, 279–294.
- Liu, M., Tolg, C., & Turley, E. (2019). Dissecting the dual nature of hyaluronan in the tumor microenvironment. *Frontiers in Immunology*, 10, 947.
- Löffler, J., Sass, F. A., Filter, S., Rose, A., Ellinghaus, A., Duda, G. N., & Dienelt, A. (2019). Compromised bone healing in aged rats is associated with impaired M2 macrophage function. *Frontiers in Immunology*, 10, 2443.
- Mahler, A., Reches, M., Rechter, M., Cohen, S., & Gazit, E. (2006). Rigid, self-assembled hydrogel composed of a modified aromatic dipeptide. *Advanced Materials*, 18, 1365–1370.
- McCloskey, A. P., Draper, E. R., Gilmore, B. F., & Laverty, G. (2017). Ultra-short self-assembling Fmoc-peptide gelators for anti-infective biomaterial applications. *Journal of Peptide Science*, 23, 131–140.
- McWhorter, F. Y., Wang, T., Nguyen, P., Chung, T., & Liu, W. F. (2013). Modulation of macrophage phenotype by cell shape. *Proceedings. National Academy of Sciences. United States of America*, 110, 17253–17258.
- Monzon, M. E., Fregien, N., Schmid, N., Falcon, N. S., Campos, M., Casalino-Matsuda, S. M., & Forteza, R. M. (2010). Reactive oxygen species and hyaluronidase 2 regulate airway epithelial hyaluronan fragmentation. *The Journal of Biological Chemistry*, 285, 26126–26134.
- Mosser, D. M., & Edwards, J. P. (2008). Exploring the full spectrum of macrophage activation. *Nature Reviews. Immunology*, 8, 958–969.
- Murray, P. J., & Wynn, T. A. (2011). Protective and pathogenic functions of macrophage subsets. *Nature Reviews. Immunology*, 11, 723–737.
- Nadernezhad, A., Forster, L., Netti, F., Adler-Abramovich, L., Teßmar, J., & Groll, J. (2020). Rheological analysis of the interplay between the molecular weight and concentration of hyaluronic acid in formulations of supramolecular HA/FmocFF hybrid hydrogels. *Polymer Journal*, 52, 1007–1012.
- Netti, F., Aviv, M., Dan, Y., Rudnick-Glick, S., Halperin-Sternfeld, M., & Adler-Abramovich, L. (2022). Stabilizing gelatin-based bioinks under physiological conditions by incorporation of ethylene-glycol-conjugated Fmoc-FF peptides. *Nanoscale*, 14, 8525–8533.
- Ni, M., Zhuo, S., Iliescu, C., So, P. T. C., Mehta, J. S., Yu, H., & Hauser, C. A. E. (2019). Self-assembling amyloid-like peptides as exogenous second harmonic probes for bioimaging applications. *Journal of Biophotonics*, 12, e201900065.
- Park, J. W., Jang, J. H., Bae, S. R., An, C. H., & Suh, J. Y. (2009). Bone formation with various bone graft substitutes in critical-sized rat calvarial defect. *Clinical Oral Implants Research*, 20, 372–378.
- Pek, Y. S., Wan, A. C., & Ying, J. Y. (2010). The effect of matrix stiffness on mesenchymal stem cell differentiation in a 3D thixotropic gel. *Biomaterials*, 31, 385–391.
- Pelham, R. J., Jr., & Wang, Y. (1997). Cell locomotion and focal adhesions are regulated by substrate flexibility. *Proceedings of the National Academy of Sciences of the United States of America*, 94, 13661–13665.
- Qiu, P., Li, M., Chen, K., Fang, B., Chen, P., Tang, Z., Lin, X., & Fan, S. (2020). Periosteal matrix-derived hydrogel promotes bone repair through an early immune regulation coupled with enhanced angiogenesis. *Biomaterials*, 227, 119552.
- Rachmiel, D., Anconina, I., Rudnick-Glick, S., Halperin-Sternfeld, M., Adler-Abramovich, L., & Sitt, A. (2021). Hyaluronic acid and a short peptide improve the performance of a PCL electrospun fibrous scaffold designed for bone tissue engineering applications. *International Journal of Molecular Sciences*, 22, 2425.
- Raeburn, J., Pont, G., Chen, L., Cesbron, Y., Lévy, R., & Adams, D. J. (2012). Fmoc-diphenylalanine hydrogels: Understanding the variability in reported mechanical properties. *Soft Matter*, 8, 1168–1174.
- Rodon Fores, J., Bigo-Simon, A., Wagner, D., Payrastra, M., Damestoy, C., Blandin, L., Boulmedais, F., Kelber, J., Schmutz, M., Rabineau, M., Criado-Gonzalez, M., Schaaf, P., & Jierry, L. (2021). Localized enzyme-assisted self-assembly in the presence of hyaluronic acid for hybrid supramolecular hydrogel coating. *Polymers*, 13, 1793.
- Ruppert, S. M., Hawn, T. R., Arrigoni, A., Wight, T. N., & Bollyky, P. L. (2014). Tissue integrity signals communicated by high-molecular weight hyaluronan and the resolution of inflammation. *Immunologic Research*, 58, 186–192.
- Seib, F. P., Prewitz, M., Werner, C., & Bornhauser, M. (2009). Matrix elasticity regulates the secretory profile of human bone marrow-derived multipotent mesenchymal stromal cells (MSCs). *Biochemical and Biophysical Research Communications*, 389, 663–667.
- Shao, A., Ling, Y., Xu, L., Liu, S., Fan, C., Wang, Z., Xu, B., & Wang, C. (2018). Xenogeneic bone matrix immune risk assessment using GGTA1 knockout mice. *Artificial Cells, Nanomedicine, and Biotechnology*, 46, S359–S369.
- Silber, J. S., Anderson, D. G., Daffner, S. D., Brislin, B. T., Leland, J. M., Hilibrand, A. S., Vaccaro, A. R., & Albert, T. J. (2003). Donor site morbidity after anterior iliac crest bone harvest for single-level anterior cervical discectomy and fusion. *Spine*, 28, 134–139.
- Smith, A. M., Williams, R. J., Tang, C., Coppo, P., Collins, R. F., Turner, M. L., Saiani, A., & Ulijn, R. V. (2008). Fmoc-diphenylalanine self assembles to a hydrogel via a novel architecture based on π - π interlocked β -sheets. *Advanced Materials*, 20, 37–41.
- Sohn, J.-Y., Park, J.-C., Um, Y.-J., Jung, U.-W., Kim, C.-S., Cho, K.-S., & Choi, S.-H. (2010). Spontaneous healing capacity of rabbit cranial defects of various sizes. *Journal of Periodontal & Implant Science*, 40, 180–187.
- Stevens, M. M. (2008). Biomaterials for bone tissue engineering. *Materials Today*, 11, 18–25.
- Sudo, H., Kodama, H. A., Amagai, Y., Yamamoto, S., & Kasai, S. (1983). In vitro differentiation and calcification in a new clonal osteogenic cell line derived from newborn mouse calvaria. *The Journal of Cell Biology*, 96, 191–198.
- Tikhonova, T., Rovnyagina, N., Arnon, Z., Yakimov, B., Efremov, Y., Cohen-Gerassi, D., Kosheleva, N., Drachev, V., Svistunov, A., Timashev, P., Adler-Abramovich, L., Shirshin, E., & Halperin-Sternfeld, M. (2021). Mechanical enhancement and kinetics regulation of Fmoc-diphenylalanine hydrogels by thioflavin T. *Angewandte Chemie (International Ed. in English)*, 60, 25339–25345.
- Tiwari, S., & Bahadur, P. (2019). Modified hyaluronic acid based materials for biomedical applications. *International Journal of Biological Macromolecules*, 121, 556–571.
- Tournier, P., Guicheux, J., Paré, A., Maltezeanu, A., Blondy, T., Veziers, J., Vignes, C., André, M., Lesoeur, J., Barbeito, A., Bardonnat, R., Blanquart, C., Corre, P., Geoffroy, V., Weiss, P., & Gaudin, A. (2021). A partially demineralized allogeneic bone graft: In vitro osteogenic potential and preclinical evaluation in two different intramembranous bone healing models. *Scientific Reports*, 11, 4907.

- Turley, E. A., Noble, P. W., & Bourguignon, L. Y. (2002). Signaling properties of hyaluronan receptors. *The Journal of Biological Chemistry*, 277, 4589–4592.
- Vacanti, J. P., & Langer, R. (1999). Tissue engineering: The design and fabrication of living replacement devices for surgical reconstruction and transplantation. *Lancet*, 354(Suppl. 1), S132–S134.
- Vegnere, R., Shestakova, I., Kalvinsh, I., Ezzell, R. M., & Janmey, P. A. (1995). Use of a gel-forming dipeptide derivative as a carrier for antigen presentation. *Journal of Peptide Science*, 1, 371–378.
- Wang, L., Gong, C., Yuan, X., & Wei, G. (2019). Controlling the self-assembly of biomolecules into functional nanomaterials through internal interactions and external stimulations: A review. *Nanomaterials*, 9, 285.
- Wang, Y., Zhang, Z., Xu, L., Li, X., & Chen, H. (2013). Hydrogels of halogenated Fmoc-short peptides for potential application in tissue engineering. *Colloids and Surfaces. B, Biointerfaces*, 104, 163–168.
- Wende, F. J., Gohil, S., Mojarradi, H., Gerfaud, T., Nord, L. I., Karlsson, A., Boiteau, J.-G., Kenne, A. H., & Sandström, C. (2016). Determination of substitution positions in hyaluronic acid hydrogels using NMR and MS based methods. *Carbohydrate Polymers*, 136, 1348–1357.
- Witzler, M., Buchner, D., Shoushrah, S. H., Babczyk, P., Baranova, J., Witzleben, S., Tobiasch, E., & Schulze, M. (2019). Polysaccharide-based systems for targeted stem cell differentiation and bone regeneration. *Biomolecules*, 9, 840.
- Woo, K. M., Chen, V. J., & Ma, P. X. (2003). Nano-fibrous scaffolding architecture selectively enhances protein adsorption contributing to cell attachment. *Journal of Biomedical Materials Research. Part A*, 67, 531–537.
- Woo, K. M., Jun, J. H., Chen, V. J., Seo, J., Baek, J. H., Ryou, H. M., Kim, G. S., Somerman, M. J., & Ma, P. X. (2007). Nano-fibrous scaffolding promotes osteoblast differentiation and biomineralization. *Biomaterials*, 28, 335–343.
- Yadav, N., Chauhan, M. K., & Chauhan, V. S. (2020). Short to ultrashort peptide-based hydrogels as a platform for biomedical applications. *Biomaterials Science*, 8, 84–100.
- Yamamoto, H., Tobisawa, Y., Inubushi, T., Irie, F., Ohyama, C., & Yamaguchi, Y. (2017). A mammalian homolog of the zebrafish transmembrane protein 2 (TMEM2) is the long-sought-after cell-surface hyaluronidase. *The Journal of Biological Chemistry*, 292, 7304–7313.
- Yang, H. C., Park, H. C., Quan, H., & Kim, Y. (2018). Immunomodulation of biomaterials by controlling macrophage polarization. *Adv. Exp. Med. Biol.*, 1064, 197–206.
- Yoshida, H., Nagaoka, A., Kusaka-Kikushima, A., Tobiishi, M., Kawabata, K., Sayo, T., Sakai, S., Sugiyama, Y., Enomoto, H., & Okada, Y. (2013). KIAA1199, a deafness gene of unknown function, is a new hyaluronan binding protein involved in hyaluronan depolymerization. *PNAS*, 110, 5612–5617.
- Zhai, P., Peng, X., Li, B., Liu, Y., Sun, H., & Li, X. (2020). The application of hyaluronic acid in bone regeneration. *International Journal of Biological Macromolecules*, 151, 1224–1239.
- Zhang, H., Yang, L., Yang, X. G., Wang, F., Feng, J. T., Hua, K. C., Li, Q., & Hu, Y. C. (2019). Demineralized bone matrix carriers and their clinical applications: An overview. *Orthopaedic Surgery*, 11, 725–737.
- Zhang, R., & Ma, P. X. (2000). Synthetic nano-fibrillar extracellular matrices with predesigned macroporous architectures. *Journal of Biomedical Materials Research. Part A*, 52, 430–438.
- Zhang, S. (2003). Fabrication of novel biomaterials through molecular self-assembly. *Nature Biotechnology*, 21, 1171–1178.
- Zhang, S., Marini, D. M., Hwang, W., & Santoso, S. (2002). Design of nanostructured biological materials through self-assembly of peptides and proteins. *Current Opinion in Chemical Biology*, 6, 865–871.
- Zhang, Y., Gu, H., Yang, Z., & Xu, B. (2003). Supramolecular hydrogels respond to ligand-receptor interaction. *Journal of the American Chemical Society*, 125, 13680–13681.
- Zhao, X.-B., Chen, Y.-P., Tan, M., Zhao, L., Zhai, Y.-Y., Sun, Y.-L., Gong, Y., Feng, X.-Q., Du, J., & Fan, Y.-B. (2021). Extracellular matrix stiffness regulates DNA methylation by PKC α -dependent nuclear transport of DNMT3L. *Advanced Healthcare Materials*, 10, 2100821.
- Zhou, M., Smith, A. M., Das, A. K., Hodson, N. W., Collins, R. F., Ulijn, R. V., & Gough, J. E. (2009). Self-assembled peptide-based hydrogels as scaffolds for anchorage-dependent cells. *Biomaterials*, 30, 2523–2530.
- Zuk, P. A., Zhu, M., Mizuno, H., Huang, J., Futrell, J. W., Katz, A. J., Benhaim, P., Lorenz, H. P., & Hedrick, M. H. (2001). Multilineage cells from human adipose tissue: Implications for cell-based therapies. *Tissue Engineering*, 7, 211–228.

SUPPORTING INFORMATION

Additional supporting information can be found online in the Supporting Information section at the end of this article.

How to cite this article: Halperin-Sternfeld, M., Pokhojaev, A., Ghosh, M., Rachmiel, D., Kannan, R., Grinberg, I., Asher, M., Aviv, M., Ma, P. X., Binderman, I., Sarig, R., & Adler-Abramovich, L. (2023). Immunomodulatory fibrous hyaluronic acid-Fmoc-diphenylalanine-based hydrogel induces bone regeneration. *Journal of Clinical Periodontology*, 50(2), 200–219. <https://doi.org/10.1111/jcpe.13725>